LBNL-45342

ERNEST ORLANDO LAWRENCE
BERKELEY NATIONAL LABORATORY

Single Well Seismic Imaging—Status Report

Thomas M. Daley, Ernest L. Majer,
and Roland Gritto

Earth Sciences Division

March 2000

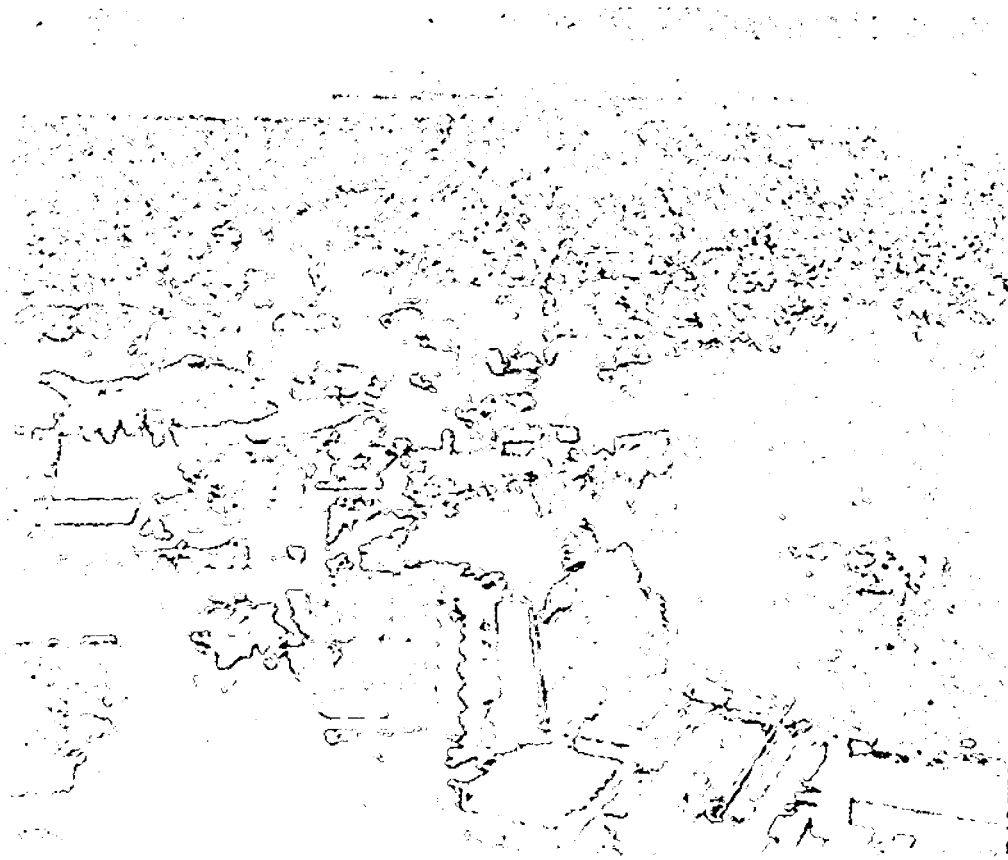

DISCLAIMER

LBNL-45342

Single Well Seismic Imaging - Status Report

Thomas M. Daley, Ernest L. Majer, and Roland Gritto

Earth Sciences Division, Lawrence Berkeley National Laboratory, Berkeley, California

March 2000

This work was supported by the Assistant Secretary for Fossil Energy, Office of Natural Gas and Petroleum Technology, the Natural Gas and Oil Technology Partnership program, of the U.S. Department of Energy under Contract No. DE-AC03-76SF000098.

Abstract. This reports updates the status of LBNL's SWSI project, including all data acquisition completed in 1999 and initial analysis of the various data sets.

1. Background

LBNL's development of SWSI technology has progressed from initial surveys using multiple cables in shallow wells to a robust, oil field scale, single cable system capable of utilizing various sources and sensors. The field testing of SWSI systems summarized and described in this report is shown in Table 1. Our first application in 1992 used a piezoelectric source and hydrophone receivers on separate cables to collect CMP data in a fractured limestone aquifer. The data successfully imaged a hydrologically significant fracture with a constant velocity CMP section (Majer, et al., 1997). Testing with a single cable in a deep well (over 1.5 km) at the MIT test site in Northern Michigan successfully acquired data in the Antrim shale section and the Niagran reef section (Daley, 1997). A DOE funded project in SWSI technology led to further testing and development of data acquisition systems.

The initial testing under the DOE project was performed at the Bayou Choctaw salt dome where an oil industry consortium was conducting experiments in salt dome imaging. Cooperation between the salt imaging consortium (SIC) and the SWSI project led to a series of field tests at the Bayou Choctaw site. The initial testing using equipment developed by CONOCO research and donated to LBNL was performed in Nov. 1997 in well #17 at Bayou Choctaw (Daley, 1998). This testing included initial tests of a tube-wave suppressor (TWS) developed by INEL, however the TWS failed by fluid leakage before usable data could be acquired. This 1997 testing used a borehole digitizer with electrical transmission of the data. The need for faster data transfer rates was apparent because the transfer time (about 1 min) was longer the acquisition time (1 to 10 seconds, depending on the source). Also, the use of an AC orbital vibrator source (Daley and Cox, 1999) required high voltage (440 v AC) power to be transmitted in the same cable as the low voltage (5 v) data signals. These concerns, plus maintenance and reliability concerns, led to replacement of the 1990 vintage electrical transmission borehole digitizer (which was originally developed by Century Geophysics, and later

modified by Conoco Inc.). The replacement borehole digitizer system used fiber optic (FO) transmission system developed in 1998 by OYO Geospace Instruments, and updated in 1999. This report will detail the field tests using the FO SWSI system beginning with tests at Texaco's test site in Humble, TX.

Table 1. Summary of LBNL SWSI Field Acquisition To Date

Year	Site	Survey Comments
1992	Conoco Oklahoma Test Site	Shallow Well with Multiple Cables
1994	MIT Michigan Test Site	Deep Well - Piezoelectric Source
1997	Bayou Choctaw Salt Dome	Multiple Sources and Sensors
1998	Texaco Humble Test Site	Fiber Optic telemetry - Orbital Vibrator Source
1998	Bayou Choctaw Salt Dome	Fiber Optic telemetry
1999	Baker-Atlas Houston Test Site	Improved Fiber Optic telemetry - TWS test
1999	Bayou Choctaw Salt Dome	Two wells, Multiple Sources and Sensors

2. SWSI - 1998

2.1. LBNL SWSI Humble Tests

Initial testing of the FO SWSI system took place in Nov 1998 at Texaco's borehole test site in Humble, Texas. This testing used the AC orbital vibrator and a 5 level 3-component wall-locking accelerometer sensor string. Data was acquired from 664 ft. to 1000 ft. at 8 ft. intervals. The source-receiver offsets were 57 to 89 ft. Figures 1a - 1e show common receiver gathers for the Humble SWSI data. The data has been deconvolved and decomposed into in-line and cross-line source polarizations (Daley and Cox, 1999). Multiple arrivals can be seen. For example, figure 1c (76 ft. offset) shows a constant velocity (about 3500 ft./s) arrival at 20 ms with highest amplitude on the vertical component. This energy is probably from a tube wave. A second arrival at

about 30 ms on the H1 component, in-line source may be a reflected arrival.

With SWSI data successfully collected using the FO acquisition system at the Humble test site, a more complete survey was planned for the Bayou Choctaw salt dome.

2.2. Bayou Choctaw SWSI Test - November 1998

After the initial SWSI data collection in 1997 at Bayou Choctaw in Well #17, which was drilled outside the salt dome in sediments, we planned a survey within the salt dome. Acquiring data within the salt dome would allow data analysis using a constant velocity medium, as well as reducing interbed reflections. We planned to acquire at least three "fans" of data over the same depth range with different source-receiver offsets, thereby allowing build up of CMP fold for imaging. With our 16 channel recording system, and 5 level 3-component sensor string, we hoped to acquire 3 fans giving 15 fold. The 3-component recordings could be "rotated" in processing to increase signal-to-noise of reflections. Well #28 was chosen (see Figure 2a) and was cleaned out prior to field operations. SWSI data was acquired using the AC orbital vibrator with a 5-level 3-component wall-locking accelerometer string. The inherent problem of tube-wave energy was addressed by increasing the source receiver offset (thereby increasing the usable time window before the tube wave arrival). Problems with the borehole digitizer and with interconnect cables limited the data acquisition. Problems with noise bursts during data recording were resolved by attaching a rubber boot to the orbital vibrator source. Apparently the source was hitting the steel casing during the source sweep and the resulting impulses traveled down the casing to the sensors. The data recorded without the source boot did not have usable signal-to-noise ratio. While no spike editing was attempted because of the number of spikes, it is possible that usable data could be recovered with more effort in data processing. The data acquired during this test is summarized in Table 2. Problems with the borehole digitizer, probably related to use of

a common electrical ground between the digitizer and the orbital vibrator power, caused the halting of data acquisition before the well survey could be completed. Other testing, such as recording with piezoelectric source and with hydrophones was also postponed.

Table 2. Bayou Choctaw, Louisiana (SMK Energy, Well #28) - Nov. 11-21, 1998 Orbital Vibrator Source (In-Line and Cross-Line Horizontal Sources)

Source Depths (Ft)	Sensors	Offsets (Min/Max)	Comments
4340 - 4267 @ 8'	5 3-C @ 8'	204' / 236'	Source Noise Bursts - No Boot
4380 - 4268 @ 8'	5 3-C @ 8'	167' / 199'	Source Noise Bursts - No Boot
4380 - 3380 @8'	3 3-C @ 8'	167' / 184'	w/ Source Boot - No Noise Burst
4364 - 3764 @8'	4 3-C @ 8' & 1 3-C @ 40'	167' / 231'	w/ Source Boot - No Noise Burst

The two data sets without noise bursts, named fan 4 and fan 5, were processed into common receiver gathers, including deconvolution and decomposition of the orbital vibrator source signal. Figure 3 shows a receiver gather for the longest offset (231 ft.) of fan 5. The tube wave arrives at about 50 ms and the data after 50 ms is dominated by tube wave reverberations. The strong arrival at 165 ms on the vertical component corresponds to a tube wave reflected from the top of the fluid column in the well. The time window before the tube wave arrival has observable energy, especially on the horizontal components. Figures 3a - 3c show the three sensors of fan 4. This data has been bandpassed 150 - 330 Hz, and enhanced with an f-x filter using a complex Weiner Levinson prediction filter 5 samples (2.5 ms) and 10 traces long. Figures 4a-4e show fan 5 with the same processing parameters.

In both fan 4 and fan 5, the vertically propagating S-wave is visible on on the horizontal components between 15 and 30 ms, depending on source-receiver offset.

Polarization of the S-wave is observable by comparing the horizontal components for each source. In a homogeneous medium, the orbital vibrator will generate a pair of orthogonal, linearly-polarized, horizontally propagating SH-mode shear waves, and this fits the observations in fan 4 and fan5. Changes in S-wave velocity as a function of depth are also observable. For instance, in figure 4b in the top left panel (in-line source, horizontal #1), the s-wave increases in arrival time from 4364 to 4244 ft. (source depth), then remains constant until the signal is lost at about 4004 ft. The observed changes in travel time correspond with velocity changes from sediment to salt (about 6000 ft./s and 8000 ft./s, respectively). Also notable on fans 4 and 5 is the disruption of coherent arrivals between about 4100 ft. and 3500 ft. This is best observed in fan 4 (Figures 3a - 3c) where the S-wave (20 -30 ms on the 4 horizontal component panels) and the tube wave (30 - 50 ms on the vertical component panels) are disrupted and incoherent over parts or all of this depth range. We believe the coupling of the borehole to the surrounding medium (salt or sediment) is responsible for the dramatic changes in direct arrival coherency (and, by implication, reflection arrival coherency). Figure 5 shows a bond log in well #28. While most of this well has poor bond (below 0.5 on figure 5), the depth range of 3650 to 4150 is particularly bad bond (less than 0.3). Realizing that both source and sensors (160 to 220 ft. below the source) are affected by borehole coupling, the bond log does correlate with spatial coherency and signal-to-noise ratio of direct arrivals.

Also observable in the common receiver gathers of fans 4 and 5 are various reflection events. Figure 6 (the 184 offset gather of figure 1c) shows three reflection events with their apparent velocities. We believe the event seen on the two horizontal components (15111, and 16000 ft./s velocities, respectively) are S-wave reflections from the change in velocity seen at 4250 (source elevation). The displayed apparent velocity is twice the actual velocity for a reflection from an interface below or above both source and receiver. These events then correspond to a true velocity of 7550 and 8000 ft./s, approximately

equal to the s-wave velocity in salt. The vertical component shows a reflection with apparent velocity of 11826 which is approximately twice the tube-wave velocity of about 6000 ft./s. This reflected tube wave appears to be a mode conversion although the direct P-wave, expected to arrive at about 10 ms, which is the most likely source for the conversion, is not visible. In fact, the orbital vibrator would be expected to have a node in radiation pattern for vertical P-waves, again assuming homogeneous media. This "reflected" tube wave, and other similar events observed in the various data sets, may be "wrap around" tube waves caused by source shots earlier in acquisition (at deeper depths) which generate tube waves reflecting up and down the borehole into the time window of later recordings.

Theses results were encouraging, although we were not able to acquire enough data in zones of good arrivals to generate CMP type imaging. Additionally, we felt the time window before tube wave arrivals needed to be increased by using larger source-receiver offsets. An important finding from this data set was that the fiber optic wireline did allow real-time multi-channel data acquisition. For the orbital vibrator source, a record length of 8 s was used, and while previous acquisition system had required up to 60 s for data transmittal, the fiber optic transmittal was done in real time, leaving only a delay of about 5 s for data storage and display.

3. SWSI - 1999

During 1999, the FO acquisition system was upgraded to the new DAS-2 version of borehole digitizer. The DAS-2 version uses two FO wires, one for data transmittal uphole and one for command transmittal downhole. The borehole digitizer was also upgraded to a maximum sample rate of 0.125 ms (8000 samples/s) with anti-alias filtering at about 95 % of the nyquist, giving usable seismic response to 3800 Hz. This extended bandwidth allows much improved recording of piezoelectric sources, and is essential to take full advantage of the relatively high Q (low attenuation) observed in

subsurface units.

3.1. SWSI Tests at Baker-Atlas

This new acquisition system was initially tested at Baker-Atlas test well B-18 in Houston, TX during Oct 1998. In this well test shots were collected with the POV (piezoelectric) source using hydrophone sensors and with the AC orbital vibrator using hydrophone and 3-component geophone sensors. The SWSI borehole system was also configured to operate a second generation tube wave suppressor developed by Idaho National Engineering and Environmental Laboratory (INEEL). This TWS uses an inflatable bladder, about 1m long, with "soft" coupling (near to borehole fluid pressure) to attenuate the tube wave energy. Figures 7a and 7b show data with the TWS inflated and deflated (respectively). The waveforms appear somewhat different because of varying background noise levels. Analysis of rms amplitudes in two time windows (60 - 140 ms, dominated by tube waves and 40 - 70 ms, dominated by P-waves) shows a decrease in tube wave energy by 3.1, but a corresponding decrease in P-wave energy by 6.6 with TWS inflation. While it is not clear why the P-wave should be attenuated, there is not distinct evidence of tube-wave suppression.

Operational tests at the Baker Atlas site were successful, leading to field experiments at Bayou Choctaw.

3.2. SWSI Preparation for Bayou Choctaw; Modeling and Crosswell Analysis

Before the SWSI survey, two studies were undertaken to guide the selection of source-receiver offset. The first was a numerical calculation of reflection (and transmission) coefficients, using Zoeppritz's equations for a salt/sediment interface at a range of incidence angles. The second was a crosswell field experiment between a well outside the salt dome and a well inside the salt dome.

The reflection coefficient solutions are shown in figures 9a-d. These solutions used the following parameters.

Salt: $Vp = 5000m/s, \quad Vs = 2667m/s, \quad \rho = 2.2x10^3 kg/m^3$

Sediment: $Vp = 2134m/s, \quad Vs = 975m/s, \quad \rho = 2.65x10^3 kg/m^3$

For our planned survey inside the salt dome, Figure 9a is most relevant. For a realistic range of incidence angles (30 - 70 degree) the P-P reflection coefficient is -0.1 to -0.3, and the SH-SH reflection coefficient is 0.35 to 0.4. The P to S conversion reflection coefficient is 0.0 to 0.4 for the various mode conversions. We expect the orbital vibrator source to generate P and SH waves predominantly (Daley and Cox, 1999), so we expect the P-SV and SH-SH events to be the strongest reflections. The incidence angle is estimate using straight rays and the interface offset distance inferred from the crosswell experiment (Figure 8). While zero source-receiver offset would give large reflection coefficients, the tube wave arrival will dominant the data. Therefor we have used larger offsets since we believe the reduction of noise (ie tube wave arrivals) will be more important than the reduction in reflection strength due to increasing incidence angle.

The crosswell field experiment was processed and analyzed to estimate the location of the salt dome edge using a constant velocity for salt and a velocity with linear vertical gradient for the sediments. The results of the crosswell experiment is shown in figure 8. The solution was only valid to about 3000 ft. depth where the sediment was inferred to intersect the well inside the salt dome. We used this result to guide our choice of source-receiver offset distance. We used straight rays and a piecewise vertical interface to model reflection arrival times in SWSI geometry for P-to-P, P-to-S and S-to-S arrivals. With an offset of 300 ft. 450 or 700 ft., we would have reflected P-to-P, P-to-S and S-to-S waves arriving before the tube wave, respectively, for the longest reflection path expected from modeling. Our final choice of offset was simply the longest possible with available equipment, as detailed below in Table #3.

3.3. SWSI Acquisition - Bayou Choctaw, October 1999

Our largest SWSI acquisition effort to date was carried out in Oct. 1999 at Well #28, we hoped to expand on the success of the 1998 acquisition. The data collection is summarized here.

Table 3. SWSI Acquisition - Well #28

Fan#	Sou/Rec	Min/Max Offsets	Depths	Interval	Stack	Comments
1	OV / Geo	473 / 513	4030-3210	10	18	with TWS
2	OV / Geo	459 / 499	3200-1500	50	4	with TWS
3	OV / Geo	293 / 333	3300 - 1500	50	2	w/o TWS
4	OV / Geo	293 / 333	4250 - 3400	10/20	8	4250-4100@10
5	POV / Geo	290 / 330	4250 - 1800	10/20	25	4250-4100@10
6	POV / Hyd	401 / 551	4040 - 1300	20	25	missing 1980-1800
7	OV / Hyd	397 / 547	1800 - 1300	20	8	
8	POV / Geo	253 / 293	3400 - 2900	20	25	Shear Mode POV

Unfortunately, these initial experiments were compromised by a problem with the DAS-2 borehole acquisition system for the 0.5 ms sample rate which was used for the OV source data (Fans 1,2,3,4 and 7). The POV data sets (recorded with 0.125 ms sample rate) were not affected by the acquisition hardware problem. Figures 11a and 11b show POV source, hydrophone receiver data from a sensor with 440 ft source-receiver offset. In Figure 11a a tube wave arrival between 80 and 110 ms is recorded at all depths with a large velocity change (5400 ft/s to 4300 ft/s) between 2600 and 2160 ft. A P-wave is observed at 28 ms arrival time (15,700 ft/s) and an S-wave is observed at 51 ms arrival time (8600 ft/s). It is notable that the P- S-wave are not observable above the background noise at all depths. Also notable is the observation that the large change in tube wave velocity does not correspond with a large change in P-wave velocity. The

speed of tube waves in a cased hole is controlled by the properties of the casing and the borehole fluid, as well as the outer rock properties. The observed change in tube wave velocity presumably is due to the change in borehole fluid bulk modulus when the fluid changes from water to oil (measured by logs at 2850 ft., see Figure 2). The change is gradational over the source-receiver separation distance (440 ft in Figure 11a). We also observe that the P-wave arrival is seen above background noise when the tube wave velocity changes at 2640 ft. This relationship is not yet understood.

The POV source was also recorded with LBNL's 3-component geophone sensors. Figure 12a shows a common receiver gather for the vertical component with a 330 ft source-receiver offset, while Figure 12b shows the horizontal components for the same offset. The 3-component sensor does give better signal-to-noise ratio for the shear-wave arrival between 3400 and 4300 (source depths) at 40ms rival time. The shear arrival is predominantly on the vertical and horizontal components. This data set (POV with 3-component geophone) has the best signal-to-noise ratio of body wave events throughout the depths surveyed. However, there is not a coherent body wave arrival at all depths surveyed. This lack of coherent body waves implies a very poor source coupling to the formation and therefor implies limited reflection imaging capability.

4. SWSI - Well #17 and #28

Because of the hardware problems associated with the 0.5 ms sampling used for orbital vibrator acquisition in well #28, Geospace Instruments agreed to reacquire the O.V. SWSI data set in well #28 and to provide a 12 level 3-component borehole system. Therefor, in Dec 1999, a second SWSI acquisition effort was carried out under LBNL supervision. Unfortunately, the seismic results were not significantly different. No coherent body waves were observed over any interval of the well, including the deeper interval in which shear-waves were observed in 1998. Additionally, the Salt Imaging Consortium provided support for Geospace to use the 12 level system with LBNL's

SWSI equipment for a survey in Bayou Choctaw Well #17. In this well, acquisition focused on the shallow section because modeling (described above) indicated reflection events would arrive earlier in the shallow section.

Table 4. SWSI Acquisition at Well #17

Fan#	Sou/Rec	Min / Max Offset	Dephs	Interval	Stack
1	OV / 3C	504 / 614	2100 -1060	10	2
2	OV / 3C	504 / 614	3200 - 2100	10	2

Figure 13 shows a shot gather from 2410 ft. (source depth). This shot gather, like others, shows no body waves and, additionally, there is evidence of "wrap around" tube wave energy. This type of tube wave energy arrives too early to be a direct (shortest distance) arrival, and is presumed to be a reverberation in the well from an earlier shot. The length of the OV sweep (9 seconds) and the cycle time between shots (12 seconds minimum) usually preclude the problem of "warp around" energy, however it is clearly a problem in the Well #17 survey. While this is a problem to be monitored in future OV SWSI efforts, the most important conclusion from the Well 17 survey is a lack of direct body wave arrivals, as mentioned above.

Following the well #17 acquisition, the "make-up" orbital vibrator survey of well #28 was conducted. Like the well #17 survey, the equipment was LBNL's cable and source with Geospace Instruments 12 level 3-C geophone sensors and FO borehole acquisition system. The source-receiver offset was reduced because of concerns about attenuation over the total propagation distance and reduction in the reflection coefficient at the increased incidence angle. The acquisition parameters are summarized in Table #5.

Table 5 SWSI Acquisition at Well #28 December 1999

Fan#	Sou/Rec	Min / Max Offset	Dephs	Interval	Stack
1	OV / 3C	258 / 368	4000 - 1500	10	4

An example shot gather of relative good quality from this survey is shown in Figure 14. A probable P-wave arrival at about 15,000 ft/s can be seen along with large amplitude tube-wave energy. In general this data set is characterized by large tube-waves, weak (or undetectable) direct body waves and insufficient signal-to-noise for reflection imaging.

5. Data Acquisition Summary

The progress of the SWSI project, with respect to data acquisition, has been very good. Multiple tests have been conducted at various well sites. The FO acquisition system has reduced noise problems. Two wells (#17 and #28) have been extensively surveyed with multiple sources and sensor combinations. Thousands of shot gathers have been collected. The ability to use high frequency piezoelectric sources or low frequency mechanical sources is important to applications in different geophysical/geological settings. Likewise, the ability to use hydrophones or 3-C clamped sensors is important to the commercial viability of the method. A survey with orbital vibrator and hydrophones can be acquired fairly quickly (less than 1 minute per station), and hydrophone strings can provide a large number of sensors. Cooperation between LBNL and Geospace Instruments has led to a flexible and expandable acquisition system. The principles are easily applied to other commercial borehole seismic systems.

Tube wave suppression remains a major problem. Integration of two versions of TWS from INEEL with the LBNL acquisition system has shown the compatibility of hardware development. However, the TWS has not been able to demonstrate enough in-field robustness to accurately determine its performance. The acquisition strategy

of increasing source-receiver offset enough to provide a low-noise time window before the initial tube-wave arrival was successful. Only the problem of "wrap around" tube waves limited this approach. The "time-window" strategy requires some knowledge of velocities and distance to target, however until tube wave suppression is improved it remains the best option. Only hardware (e.g. extension cables) and other acquisitions concerns (e.g. how to place long cables into the well) limit the viability of this method. Varying the source-receiver offset with interconnecting extension cables is also a way to increase CMP fold coverage.

We believe that poor well casing bond has limited the data quality in well #28. This is clearly an important factor in source coupling. The high frequency piezoelectric source coupled better than the low frequency orbital vibrator source, thereby providing more coherent direct arrivals. The beneficial aspects of well #28 (ie location in a relatively homogeneous medium near a sub-vertical interface) were apparently wasted because not enough energy was transmitted into the media.

The success of SWSI acquisition developments is at the point where our efforts are focused on finding a well site which can be better used for imaging, and testing of imaging algorithms. The ability to acquire the data is no longer in question.

6. CMP Analysis

Despite the generally poor data quality and lack of coherent direct arrivals in the well 17 and well 28 surveys, we decided to try common midpoint (CMP) stacks of the various SWSI data sets. A range of velocities was used to image the P-wave, S-wave, and P-to-S converted reflections. We used a suite of stacking velocities from 5000 ft/s to 20,000 ft/s at 500 ft/s intervals. Figures 15a and 15b show constant velocity (cv) stacks at 8000 ft/s and 15000 ft/s for data between 10 and 70 ms (the reflection time window) from the POV and hydrophone data set. Estimated reflection times (from crosswell modeling described above) are plotted on the sections. While there are interesting

events observable (such as at 12 ms from 3000 to 3400 ft, and at 32 ms from 3200 to 4000 ft), we do not believe data quality supports interpretation at this time. Figures 16a - 16d show cv stacks for the POV and geophone data set. Again, we do not believe data quality supports interpretation.

7. Summary

The SWSI project has made large strides in data acquisition. Acquisition can now be planned with the assumption that a complete data set will be obtained. Four different combinations of source and receivers have been used to survey at multiple well sites. The focus of recent work has been imaging of a salt dome flank. Within this context we have investigated the reflection coefficients expected, and the source-receiver offsets which maximize the imaging quality. Development of a tube-wave suppressor remains an important goal. Initial tests of the INEEL TWS have been inconclusive, but the data has been too limited for an accurate assessment. The strategy of increasing source-receiver offset to open a reflection time-window before the tube-wave arrival appears to be successful. We believe poor source coupling at the Bayou Choctaw wells has limited the data quality to date. The clear body waves observed at the Humble test site and at the bottom of Bayou Choctaw well #28 could not be observed in the rest of well #28, and the body waves had very poor signal-to-noise ratio in well #17. During 2000 we will continue to try and improve the imaging of SWSI data from wells 17 and 28. We shall also be attempting to find a new well site which is known to be well coupled to the formation and which has a suitable target for the SWSI technique.

8. Acknowledgments

This work was supported by the Assistant Secretary for Fossil Energy, Office of Natural Gas and Petroleum Technology, the Natural Gas and and Oil Technology Partnership program, of the U.S. Department Energy under Contract No. DE-AC03-

76SF00098. Thanks to all the field personnel of LBNL and to the members of the Salt Imaging Consortium.

9. Disclaimer

References

Daley, T.M. and Cox, D., Orbital vibrator seismic source for simultaneous P- and S-wave crosswell acquisition, Geophysics (submitted 5/99).

Daley, T.M., Single Well Seismic Imaging Tests: Nov 1997 at Bayou Choctaw Site, LBNL Report #42672, Lawrence Berkeley National Laboratory, February 1998.

Daley, T.M., Single Well Seismic Imaging in a Deep Borehole using a piezoelectric Orbital Vibrator, LBNL Report #42673, Lawrence Berkeley National Laboratory, June 1997.

Majer, E.L., Peterson, J.E., Daley, T.M., Kaelin, B., Queen, J., D'Onfro, P., and Rizer. W, Fracture Detection using Crosswell and Single Well Surveys, *Geophysics*, v62, n2, 1997.

This manuscript was prepared with the AGU LaTeX macros v3.0.

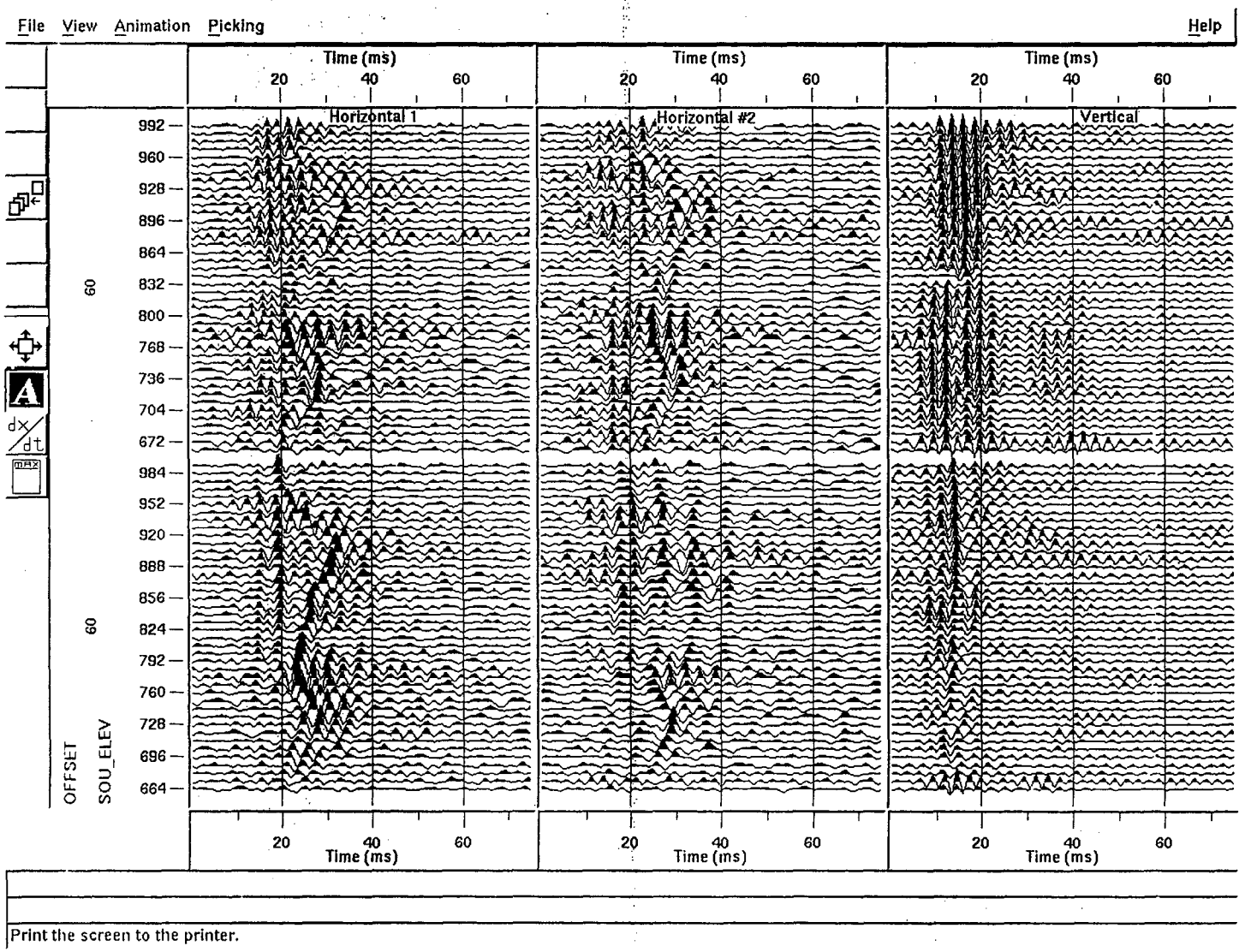

Figure 1a Common receiver gather from Humble test site for a 3-component sensor with at 60 ft. source-receiver offset. The three panels show the three components (horizontal, horizontal, vertical) for two the two polarizations of the orbital vibrator. A direct arrival is observed at about 10 ms on the vertical, and a combination of reflected or diffracted energy is seen between 20 and 40 ms on the horizontal components.

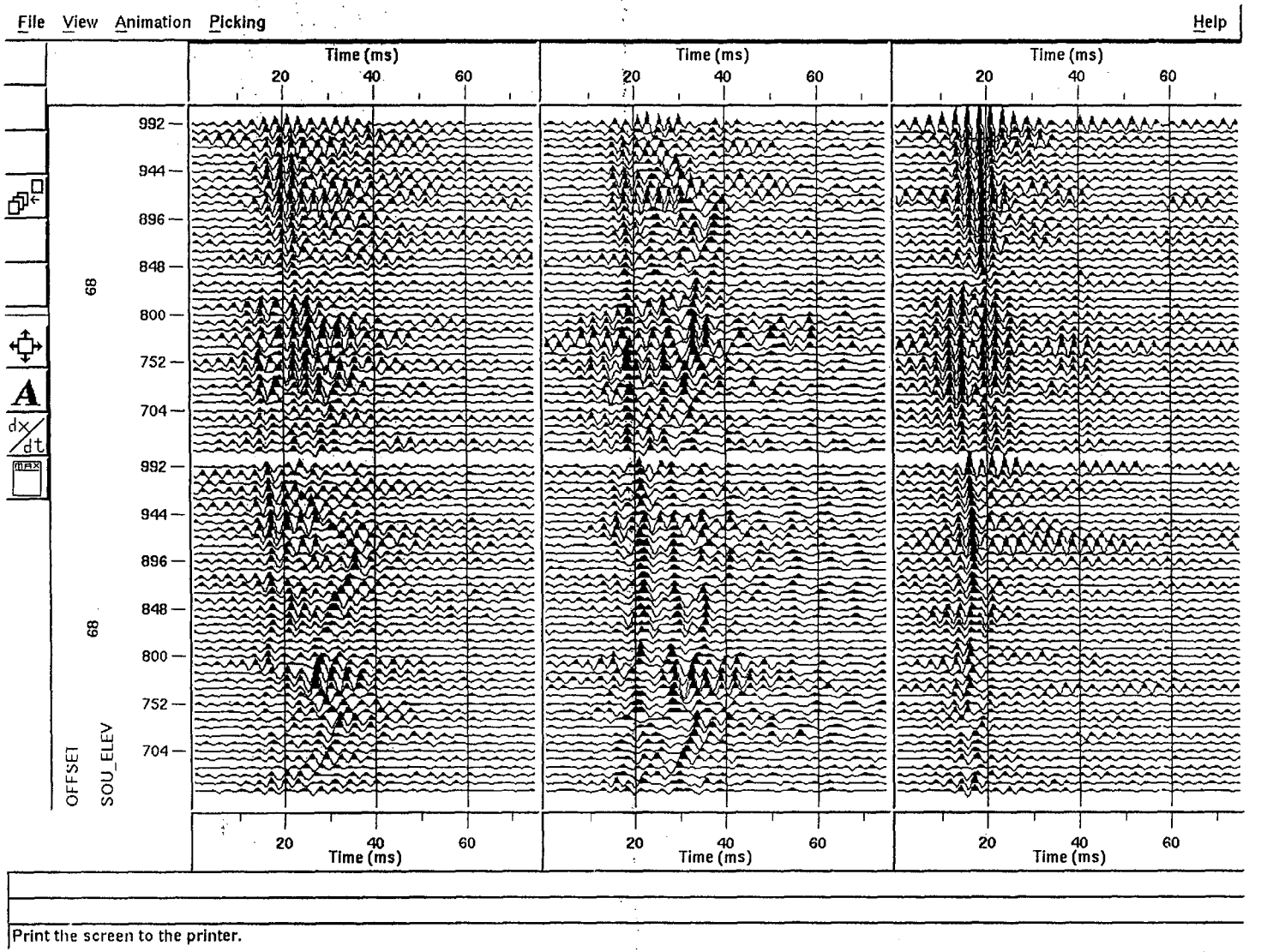

Figure 1b Common receiver gather from Humble test site for a 3-component sensor with at 68 ft. source-receiver offset. The three panels show the three components (horizontal, horizontal, vertical) for two the two polarizations of the orbital vibrator.

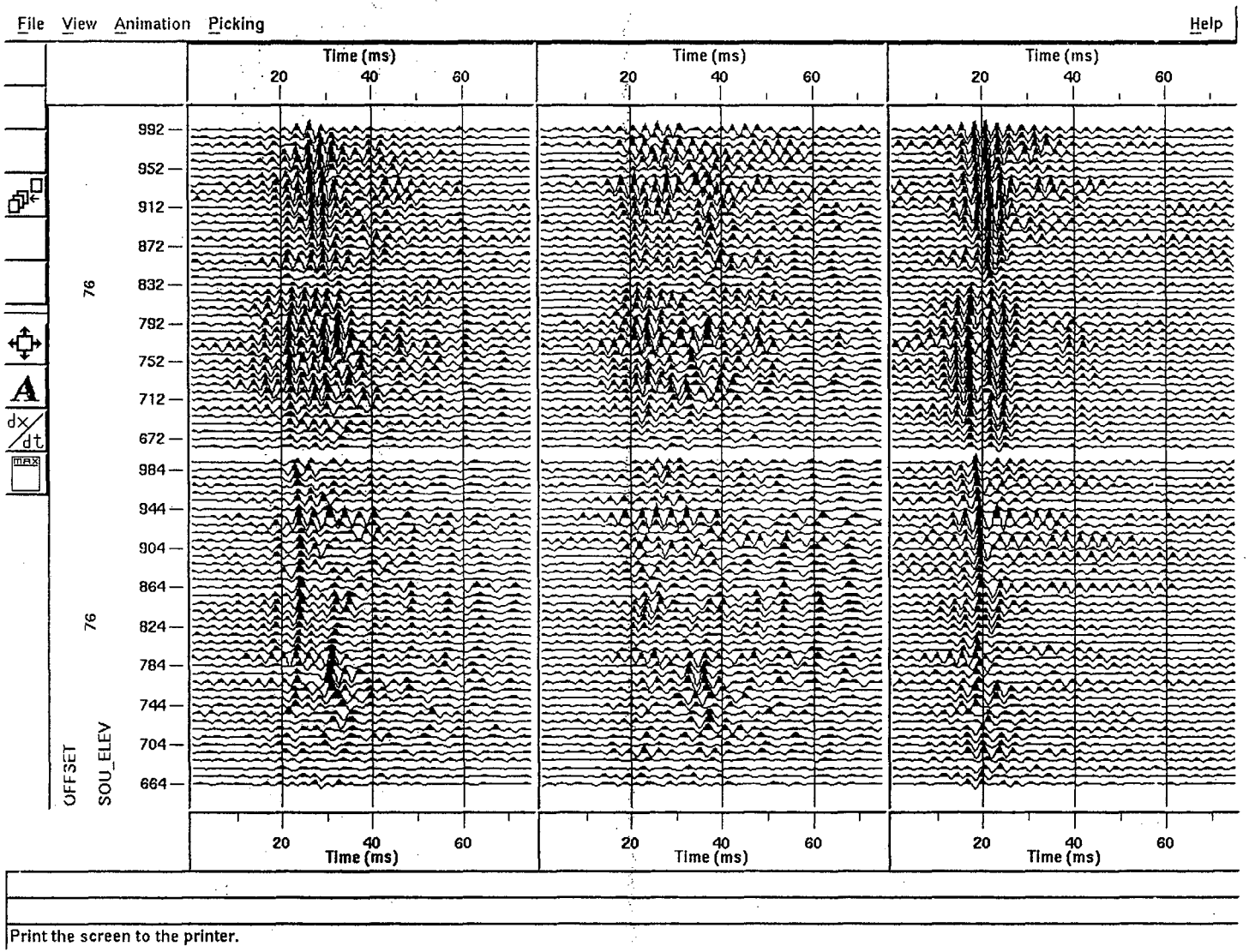

Figure 1c Common receiver gather from Humble test site for a 3-component sensor with at 76 ft. source-receiver offset. The three panels show the three components (horizontal, horizontal, vertical) for two the two polarizations of the orbital vibrator.

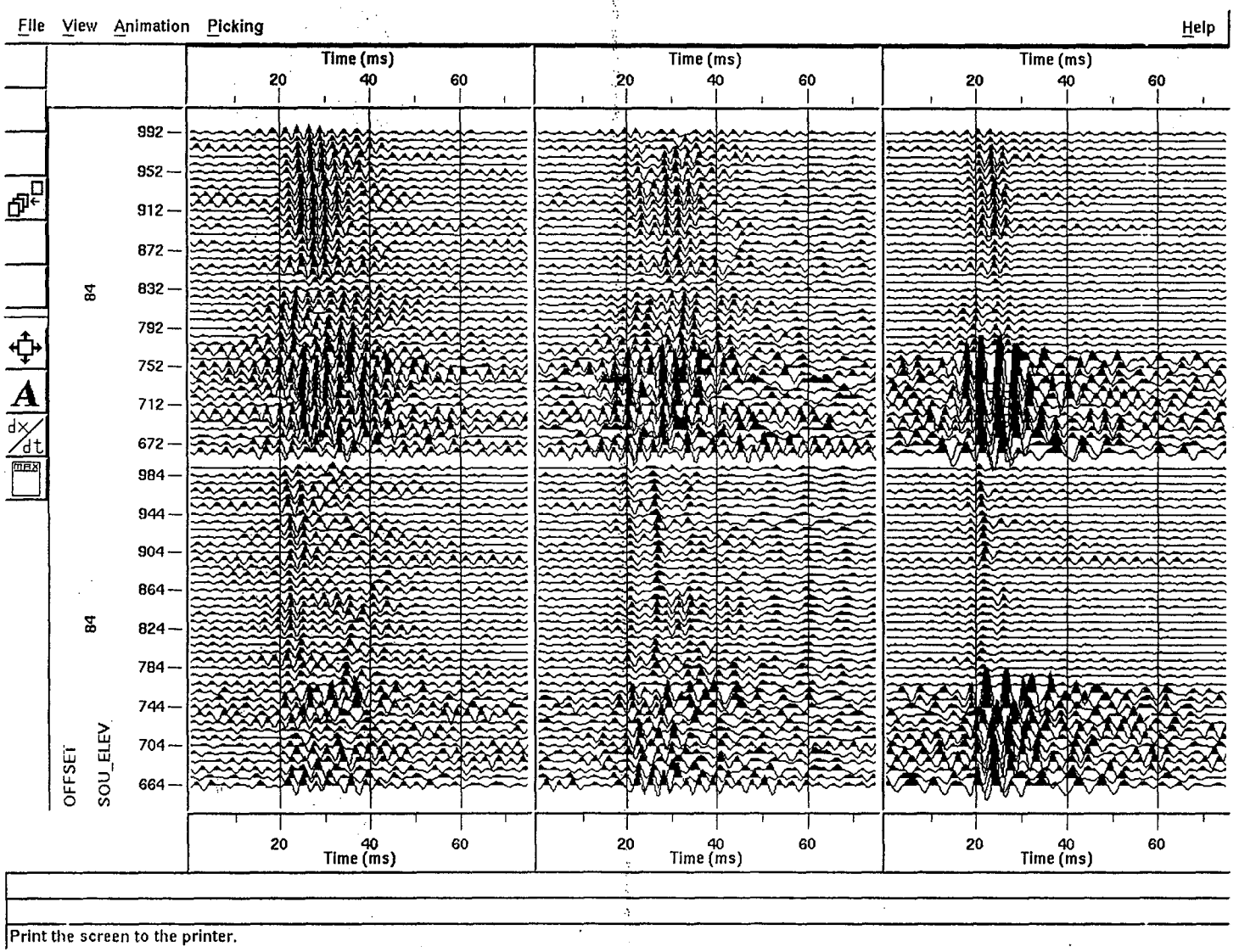

Figure 1d Common receiver gather from Humble test site for a 3-component sensor with at 84 ft. source-receiver offset. The three panels show the three components (horizontal, horizontal, vertical) for two the two polarizations of the orbital vibrator.

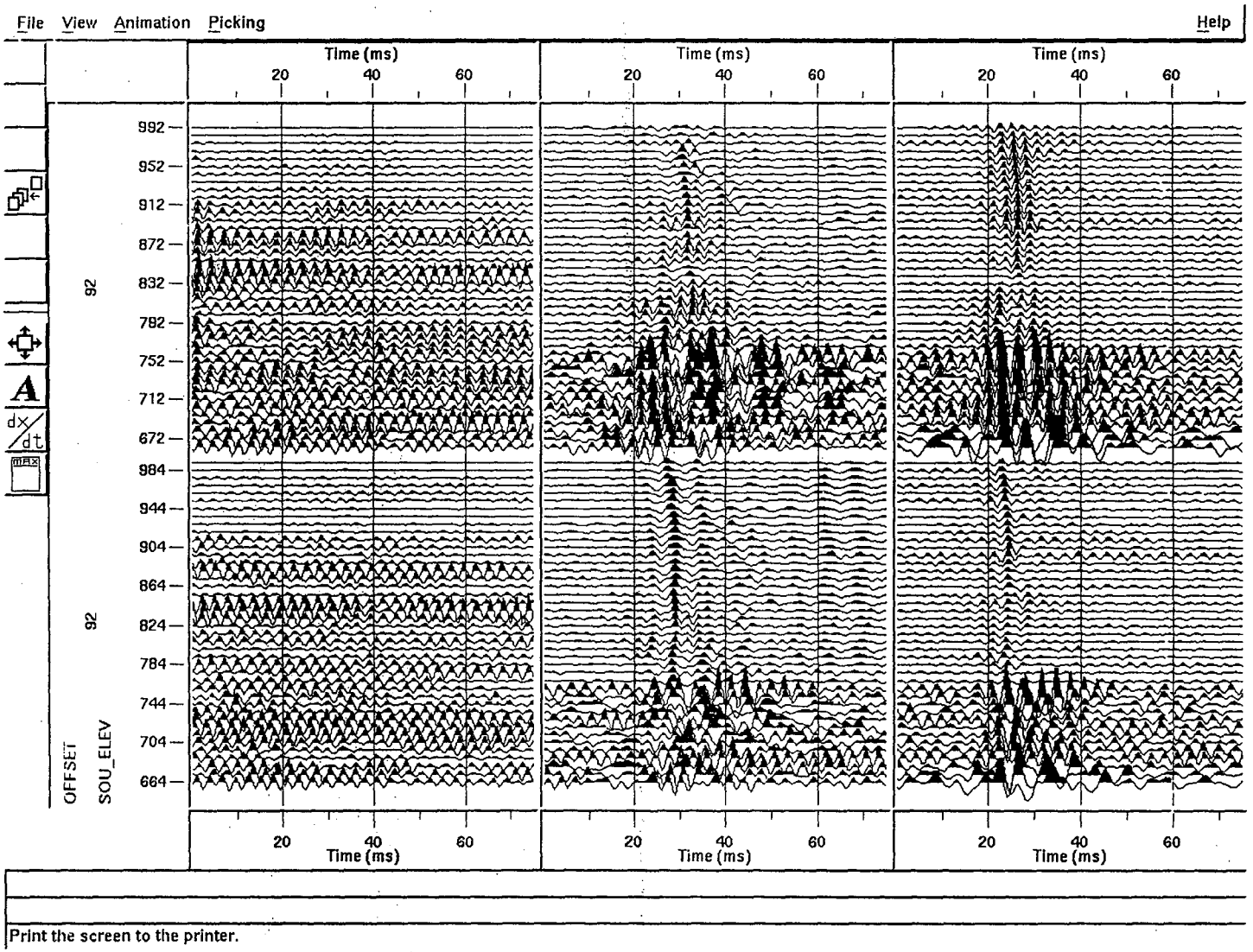

Figure 1e Common receiver gather from Humble test site for a 3-component sensor with at 92 ft. source-receiver offset. The three panels show the three components (horizontal, horizontal, vertical) for two the two polarizations of the orbital vibrator.

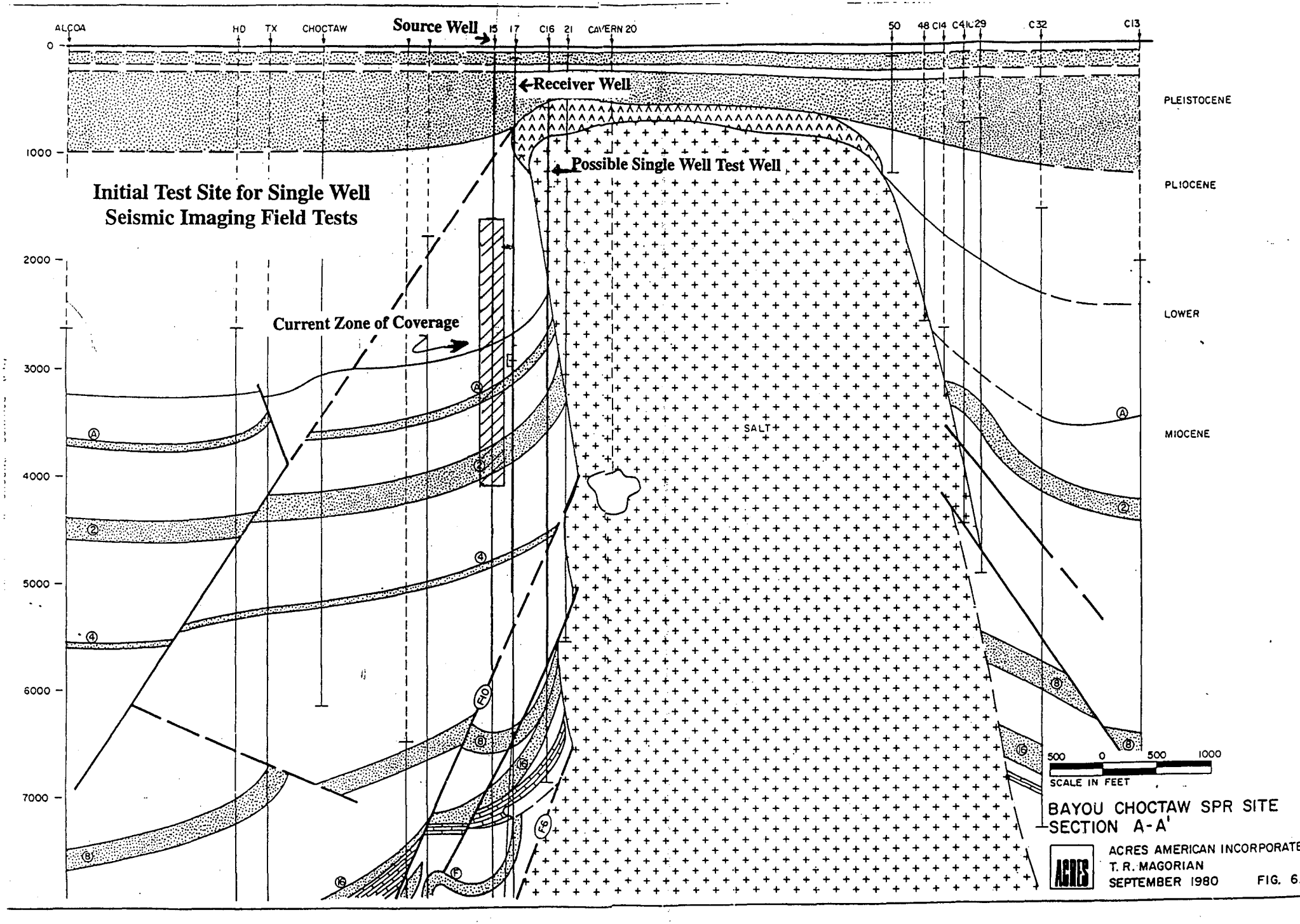

Figure 2a Location map for Bayou Choctaw salt dome.

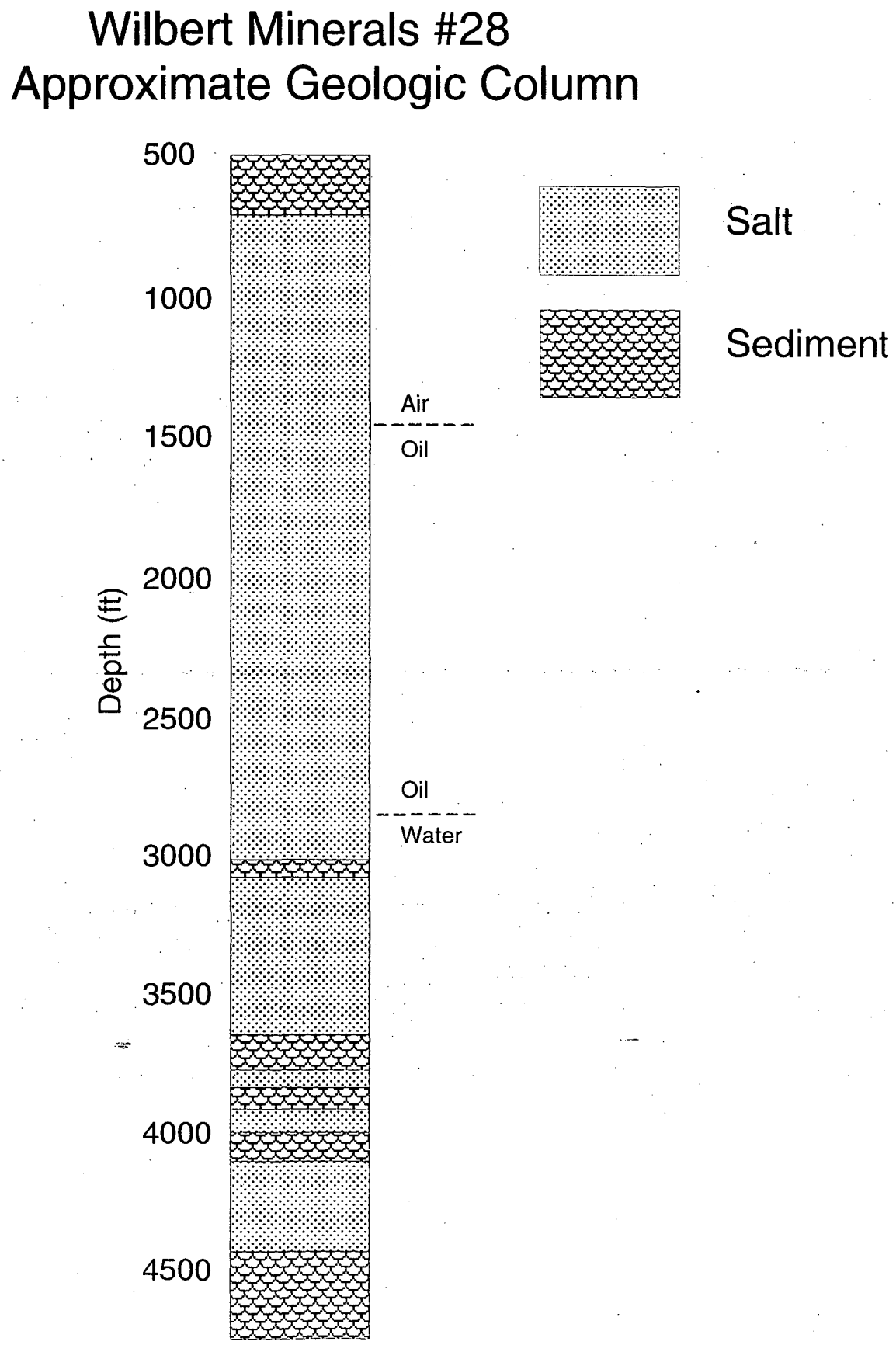

Figure 2b. Approximate geologic section for well \#28 showing salt and sediment sections and borehole fluid.

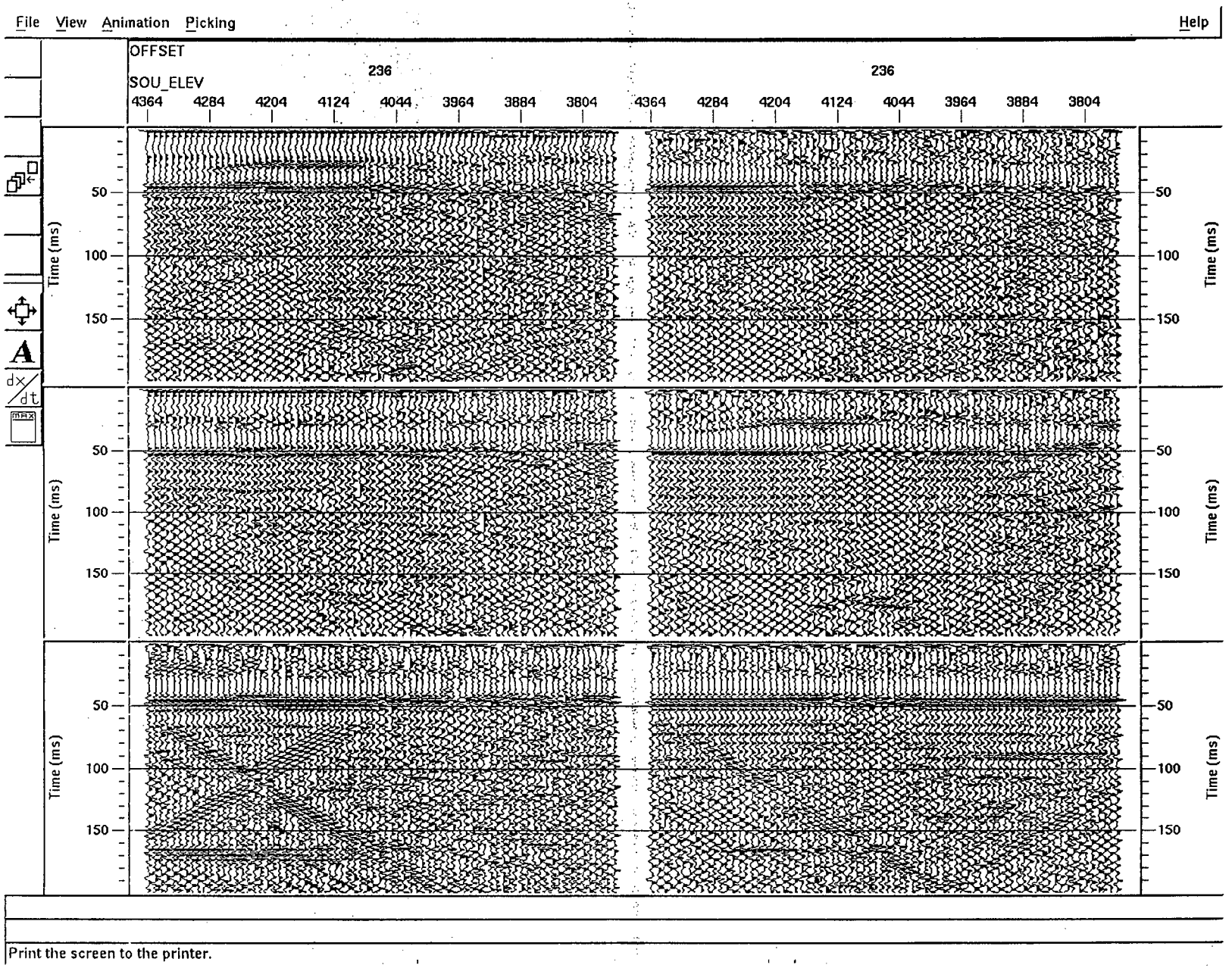

Figure 3 Common receiver gather from well \#28 for a 3-component sensor with at 236 ft. source-receiver offset. The three panels show the three components (horizontal, horizontal, vertical) for two the two polarizations of the orbital vibrator. A shear-wave arrival can be seen between 20 and 30 ms on the horizontal components. Tube wave reverberations are

Fig 4

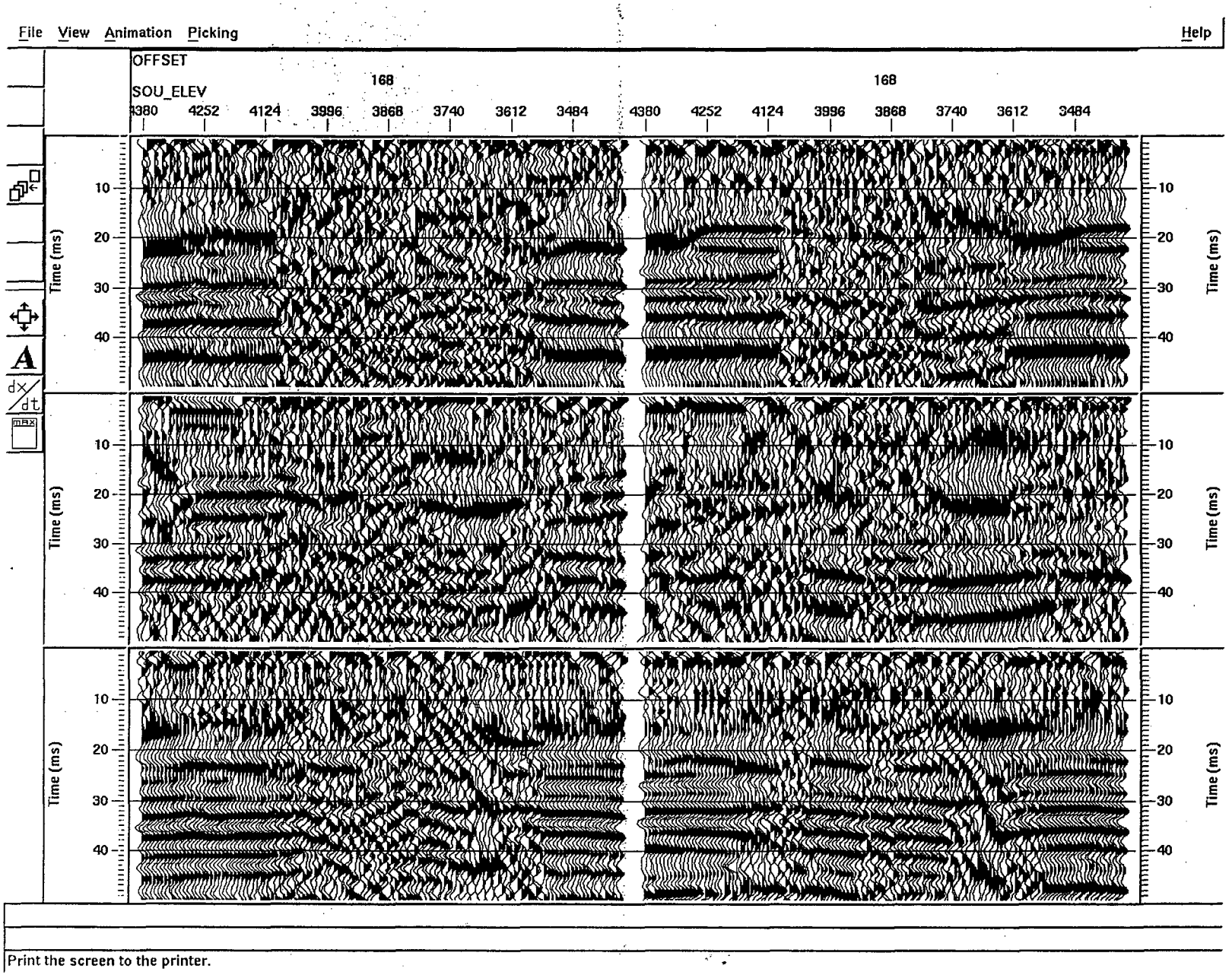

Figure 3a Common receiver gather from well \#28 for a 3-component sensor with at 168 ft. source-receiver offset. The three panels show the three components (horizontal, horizontal, vertical) for two the two polarizations of the orbital vibrator.

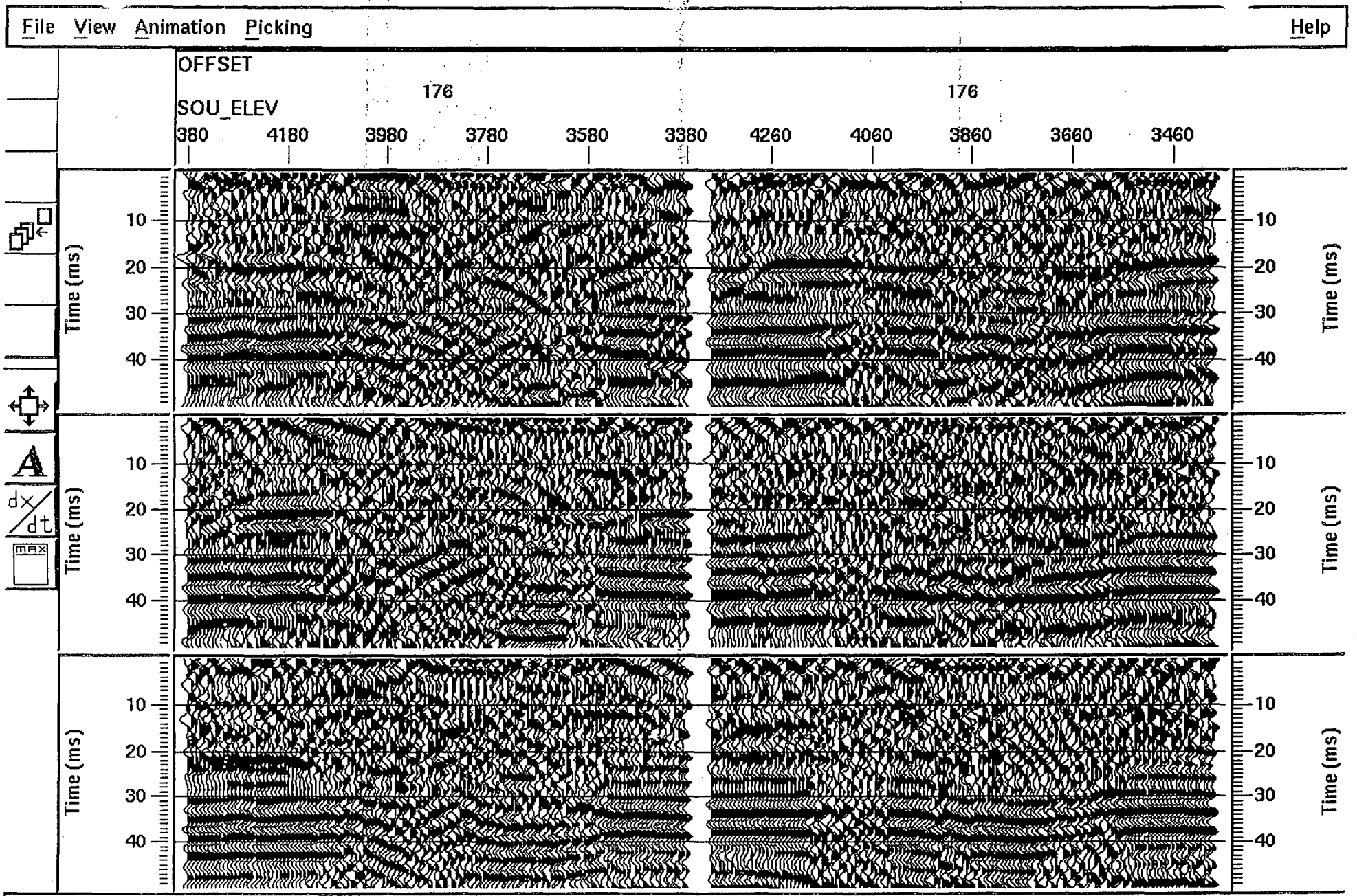

Print the screen to the printer.

Figure 3b Common receiver gather from well \#28 for a 3-component sensor with at 176 ft. source-receiver offset. The three panels show the three components (horizontal, horizontal, vertical) for two the two polarizations of the orbital vibrator.

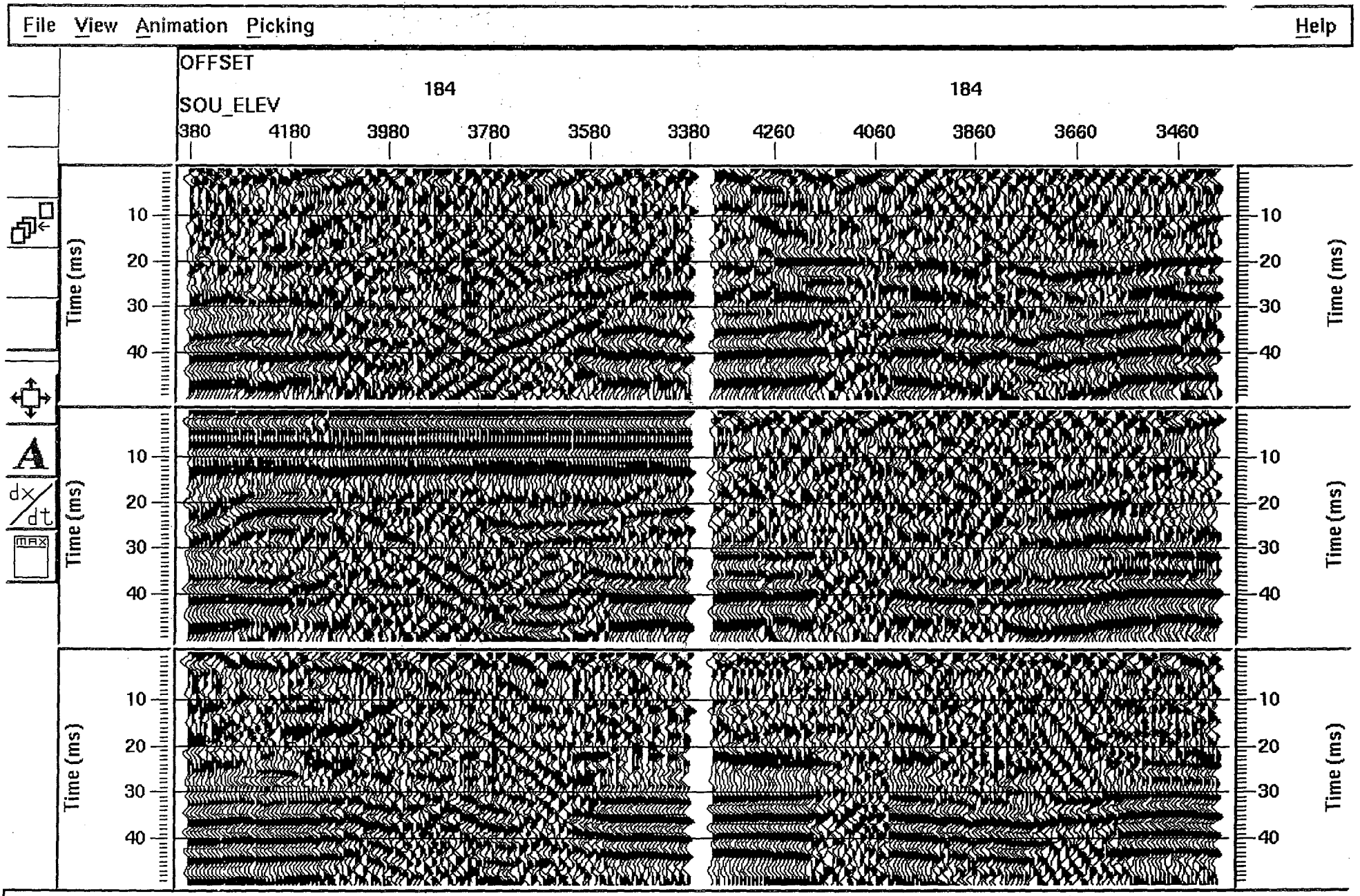

Print the screen to the printer.

Figure 3c Common receiver gather from well \#28 for a 3-component sensor with at 184 ft. source-receiver offset. The three panels show the three components (horizontal, horizontal, vertical) for two the two polarizations of the orbital vibrator.

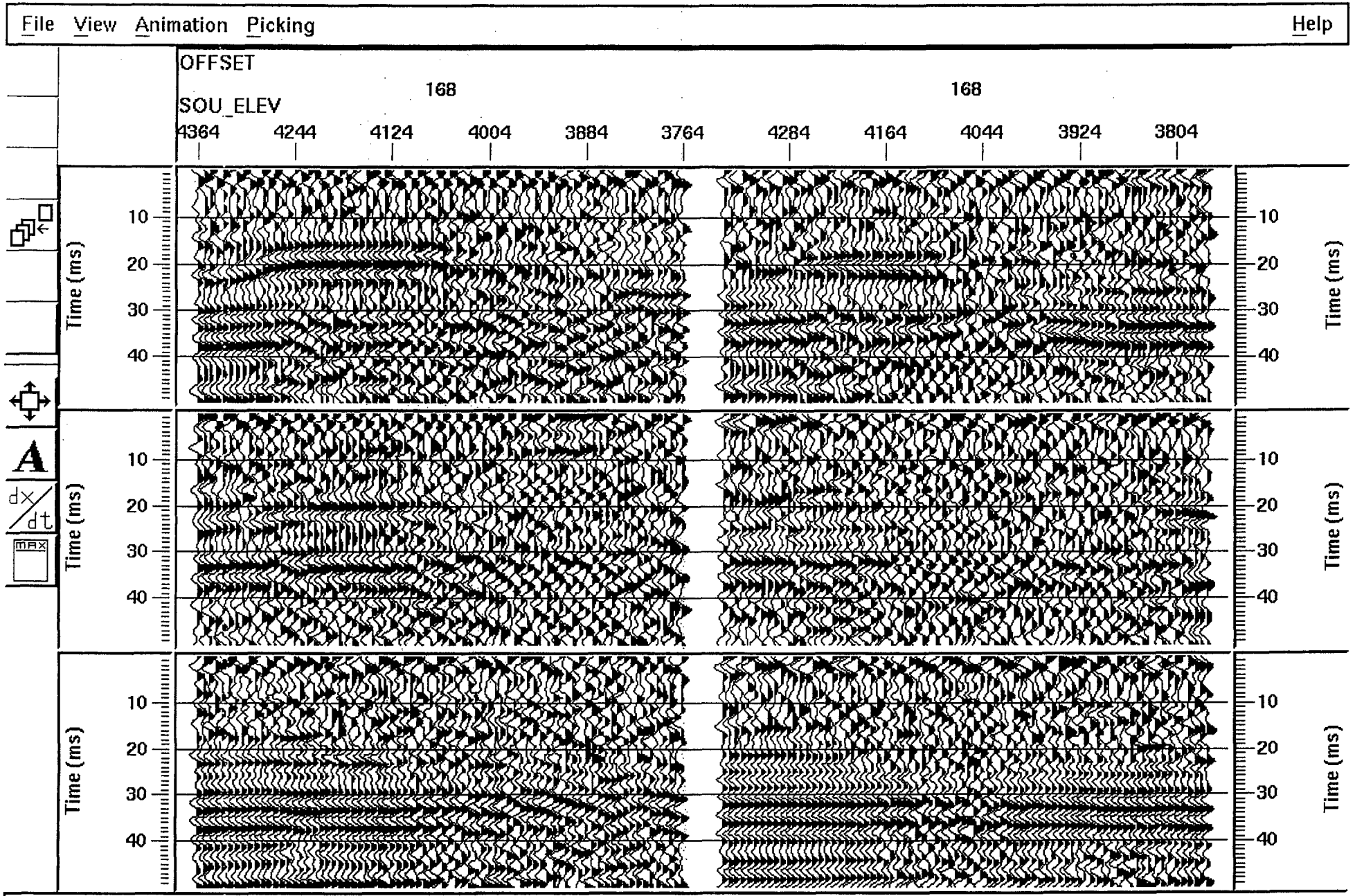

Print the screen to the printer.

Figure 4a Common receiver gather from well \#28 for a 3-component sensor with at 168 ft. source-receiver offset. The three panels show the three components (horizontal, horizontal, vertical) for two the two polarizations of the orbital vibrator

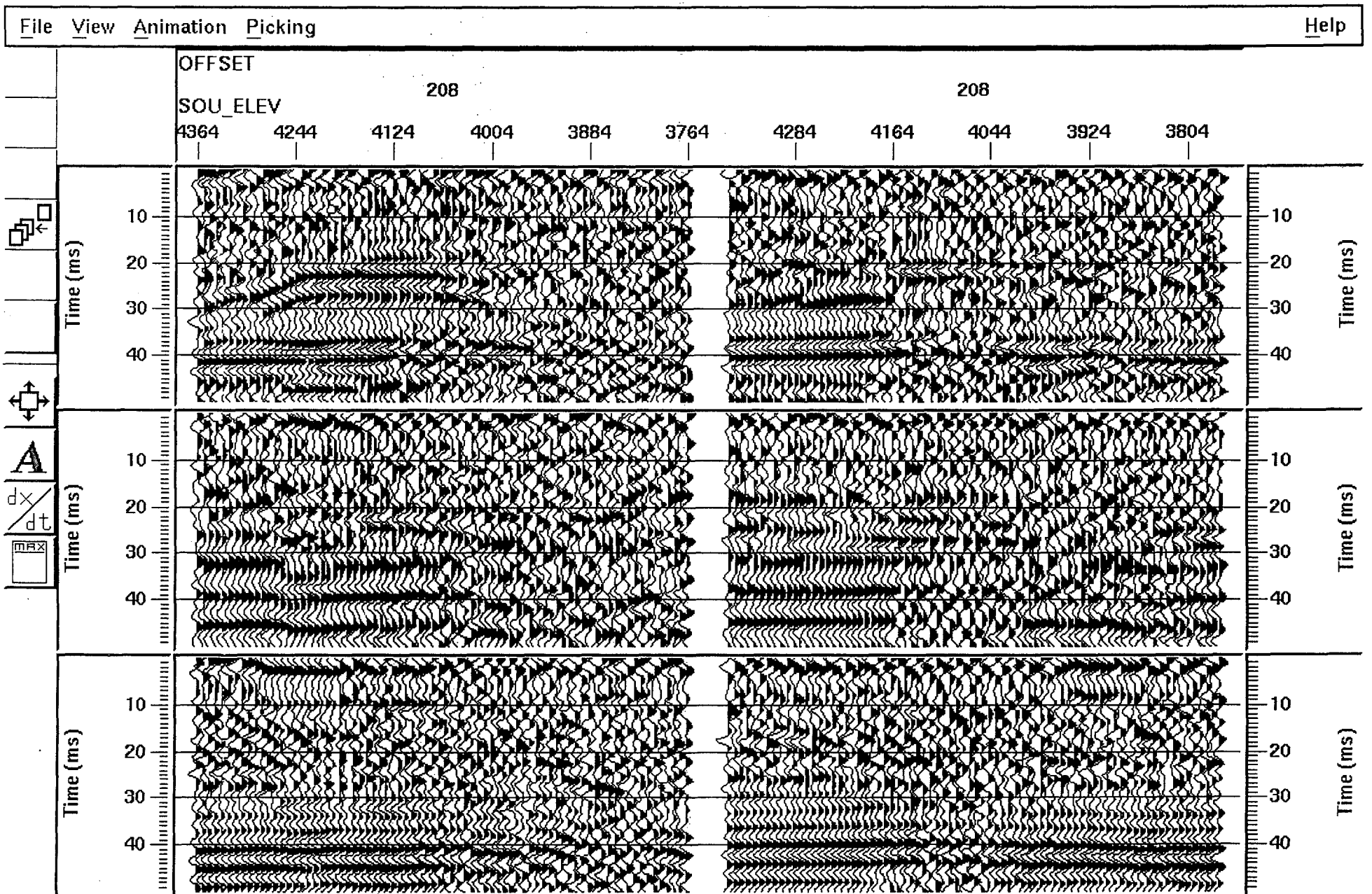

Print the screen to the printer.

Figure 4b Common receiver gather from well \#28 for a 3-component sensor with at 208 ft. source-receiver offset. The three panels show the three components (horizontal, horizontal, vertical) for two the two polarizations of the orbital vibrator.

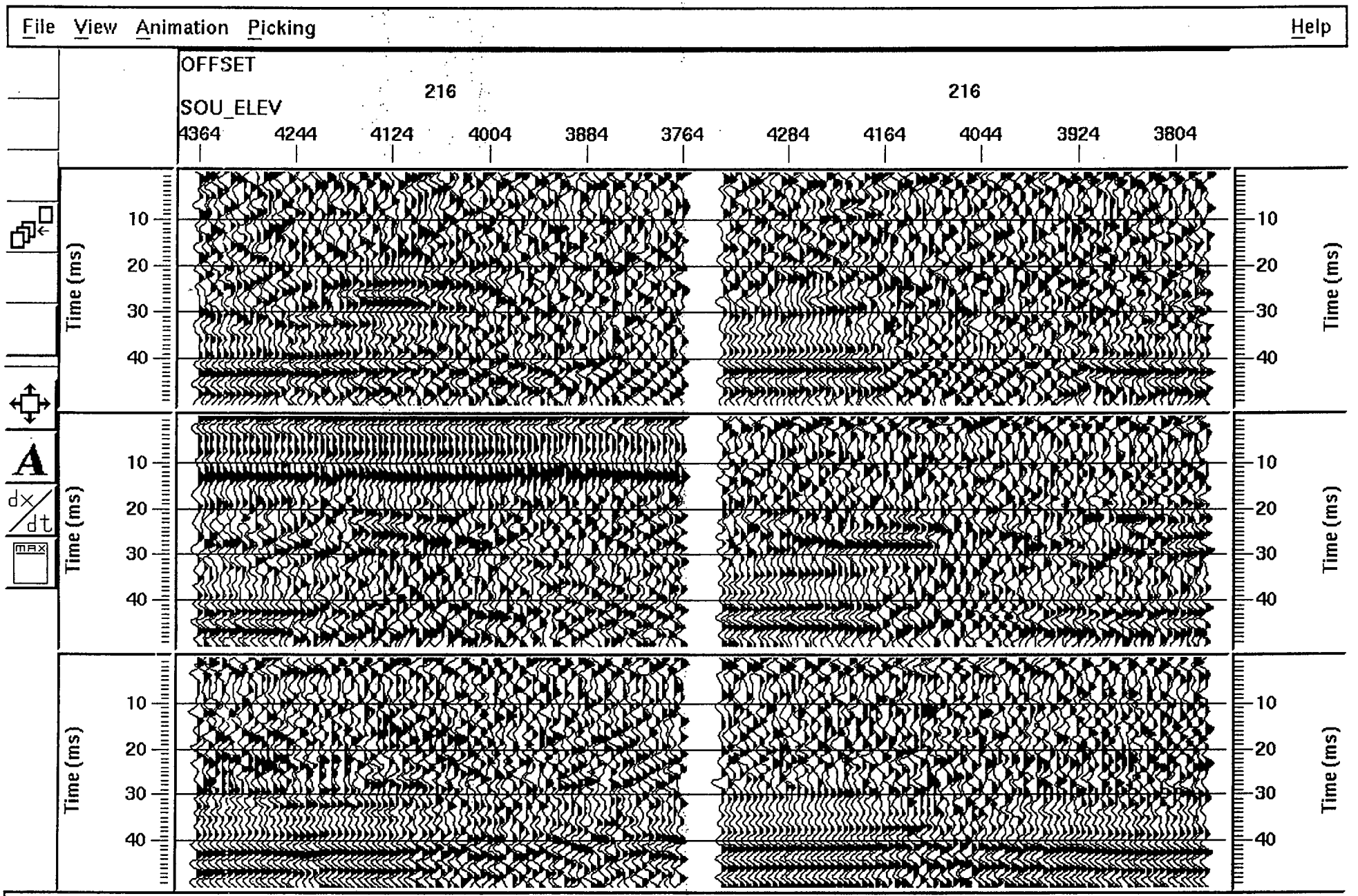

Print the screen to the printer.

Figure 4c Common receiver gather from well \#28 for a 3-component sensor with at 216 ft. source-receiver offset. The three panels show the three components (horizontal, horizontal, vertical) for two the two polarizations of the orbital vibrator.

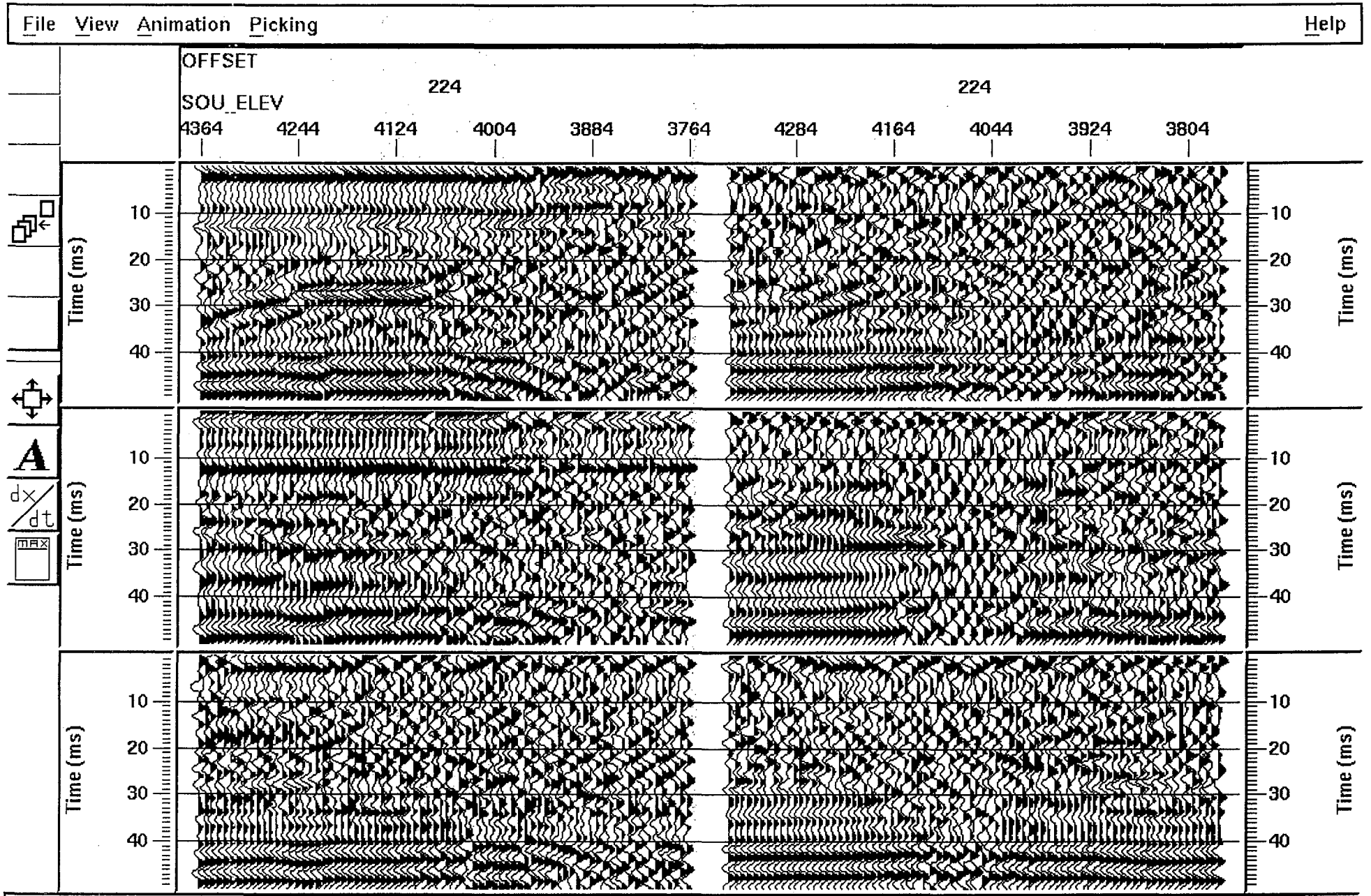

Figure 4d Common receiver gather from well \#28 for a 3-component sensor with at 224 ft. source-receiver offset. The three panels show the three components (horizontal, horizontal, vertical) for two the two polarizations of the orbital vibrator.

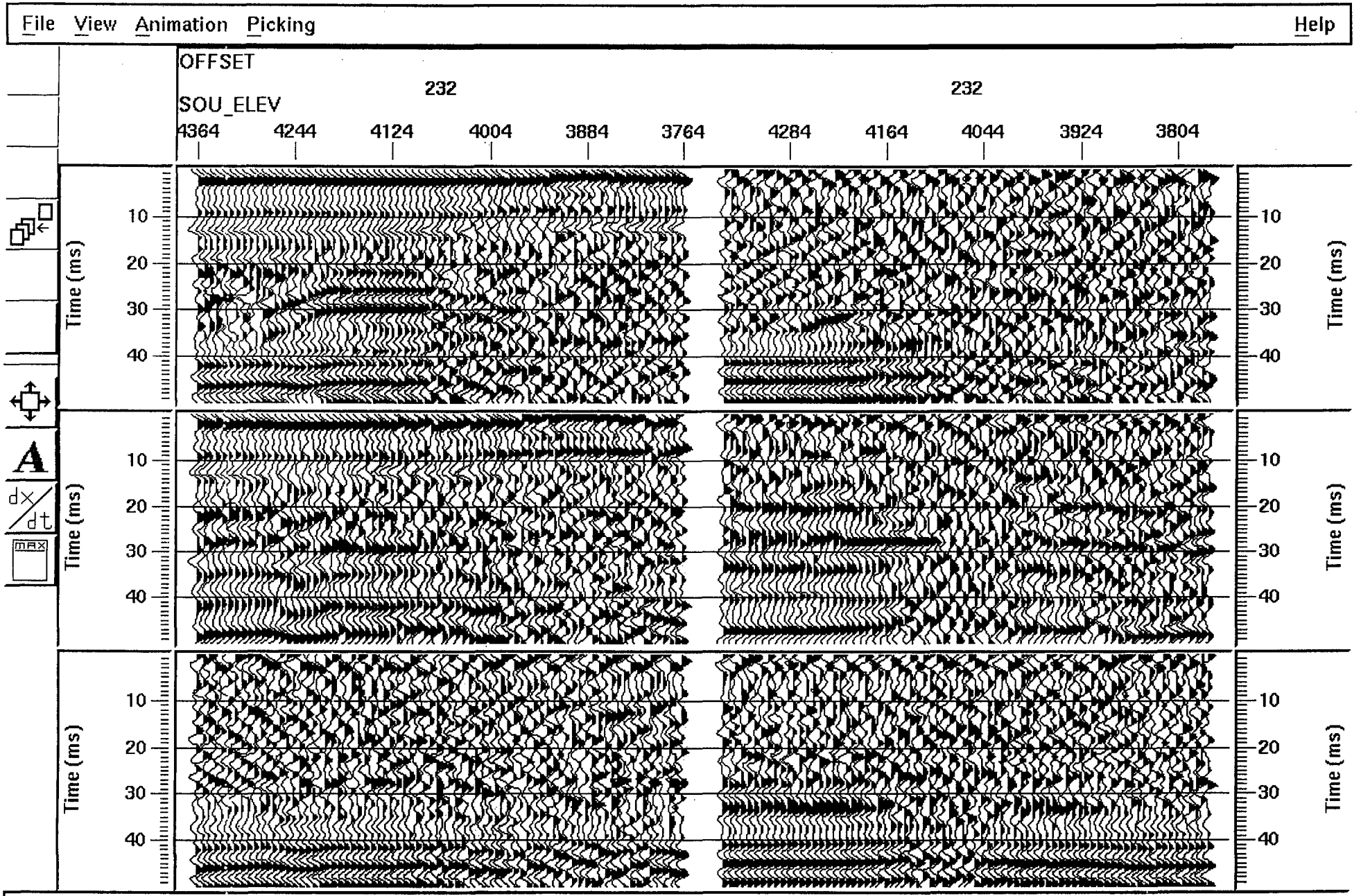

Print the screen to the printer.

Figure 4e Common receiver gather from well \#28 for a 3-component sensor with at 232 ft. source-receiver offset. The three panels show the three components (horizontal, horizontal, vertical) for two the two polarizations of the orbital vibrator.

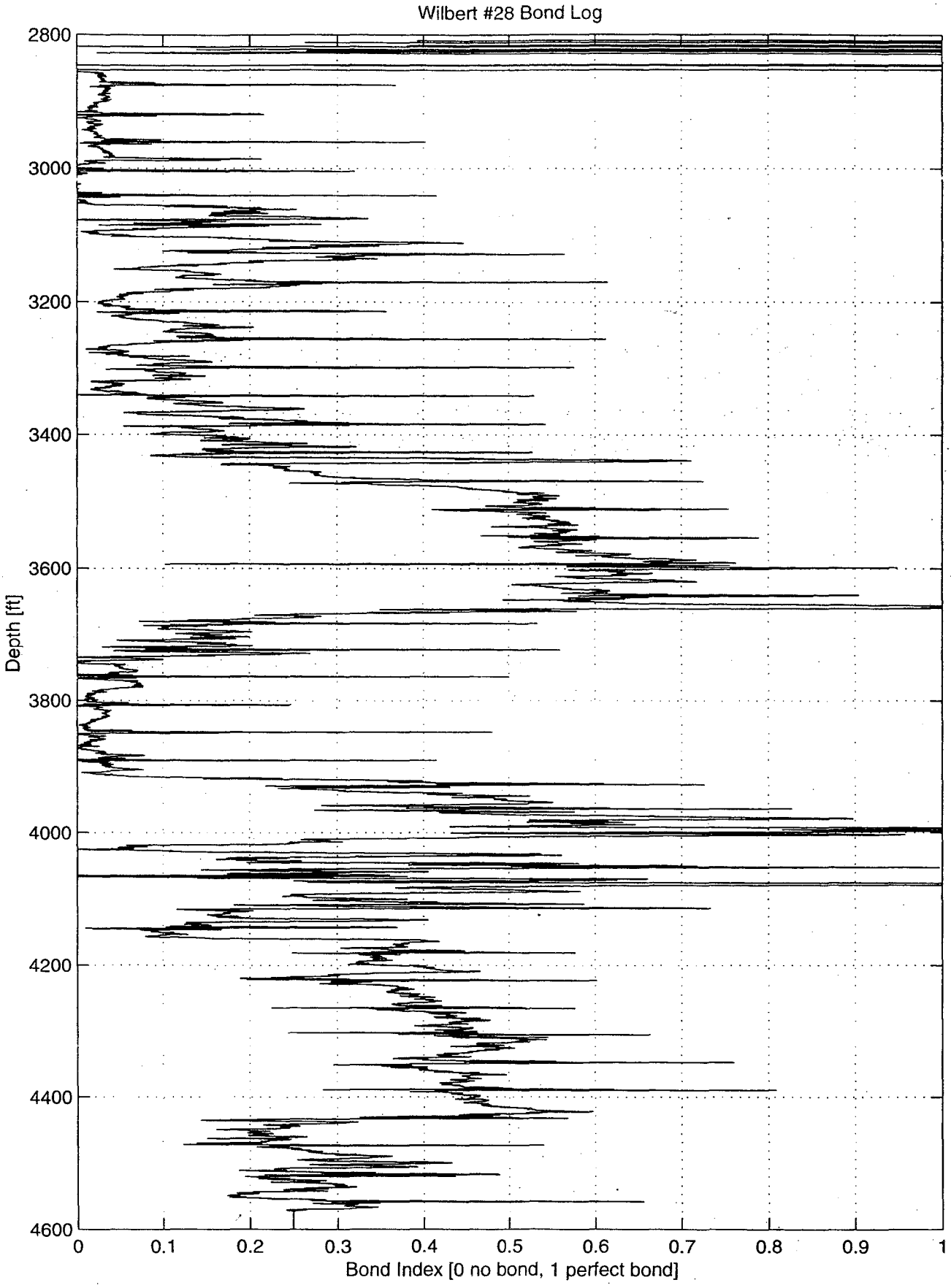

Figure 5 Bond log for well \#28.

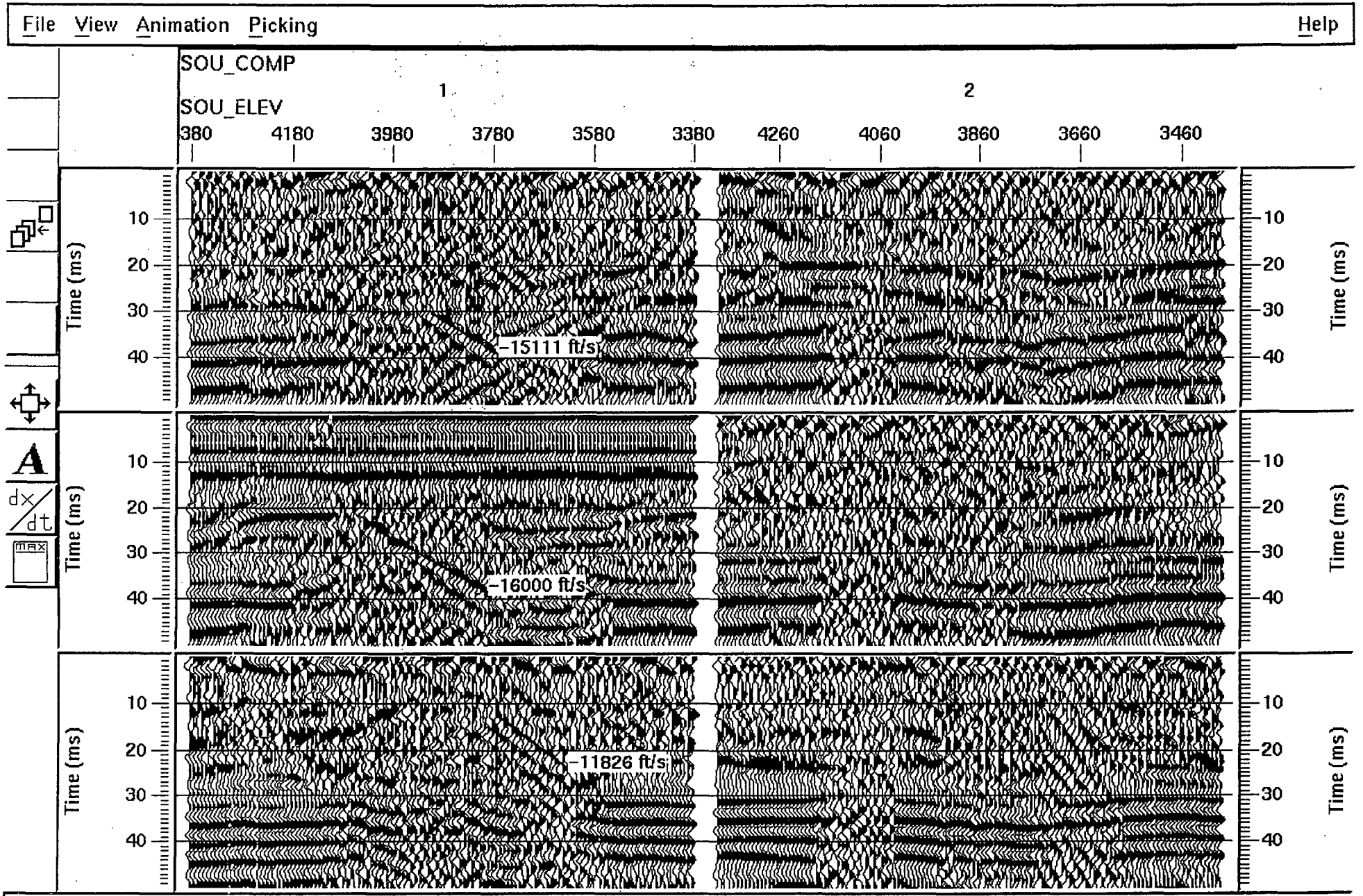

Print the screen to the printer.

Figure 6 Common receiver gather from well \#28 for a 3-component sensor with at 184 ft. source-receiver offset. The three panels show the three components (horizontal, horizontal, vertical) for two the two polarizations of the orbital vibrator. The apparent velocity of three reflection events has been labeled on the plot. For a horizontal reflector, the apparent velocity will be twice the true velocity. We interpret these events as reflected S-wave on the horizontal components, and reflected tube wave on the vertical component.

Baker Atlas 500' source depth

Tube Wave Suppressor Inflated

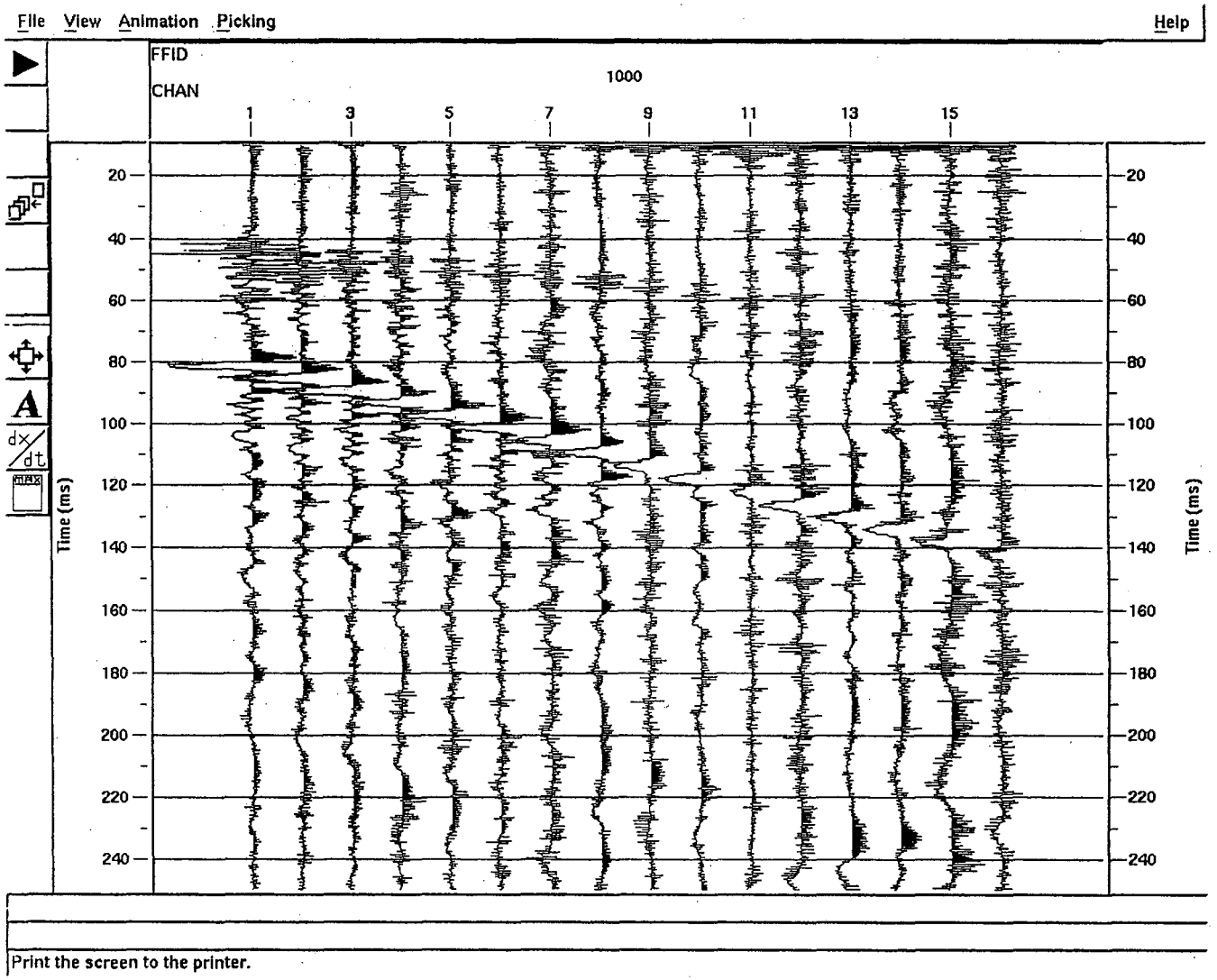

Figure 7a Shot gather for data from Baker-Atlas test well B-18 with the INEEL tube wave suppressor inflated. The direct P-wave (40 - 60 ms) and tube-wave (80 - 140 ms) are observed.

Tube Wave Supressor deflated

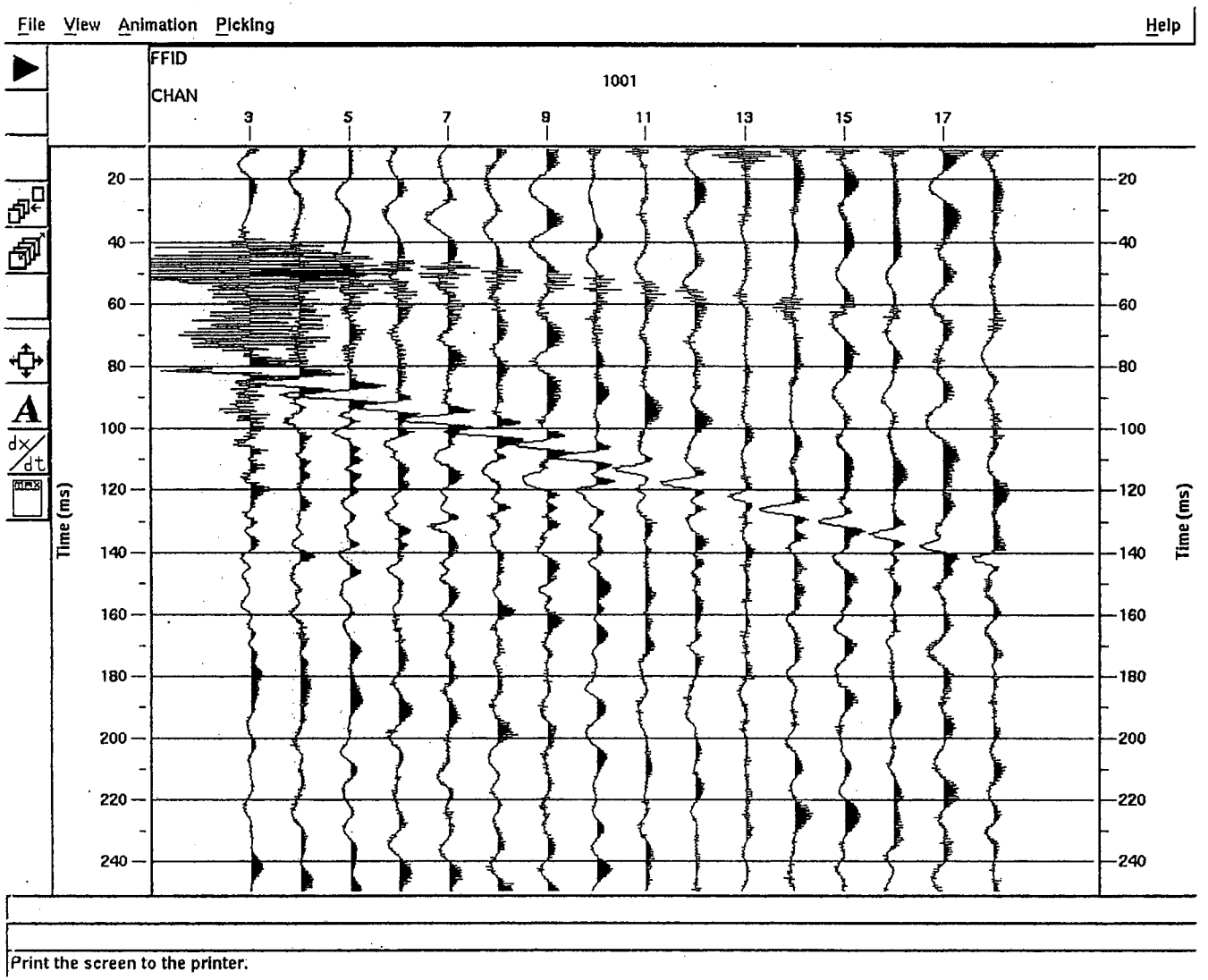

Figure 7b Shot gather for data from Baker-Atlas test well B-18 with the INEEL tube wave suppressor deflated. The direct P-wave (40 - 60 ms) and tube-wave (80 - 140 ms) are observed.

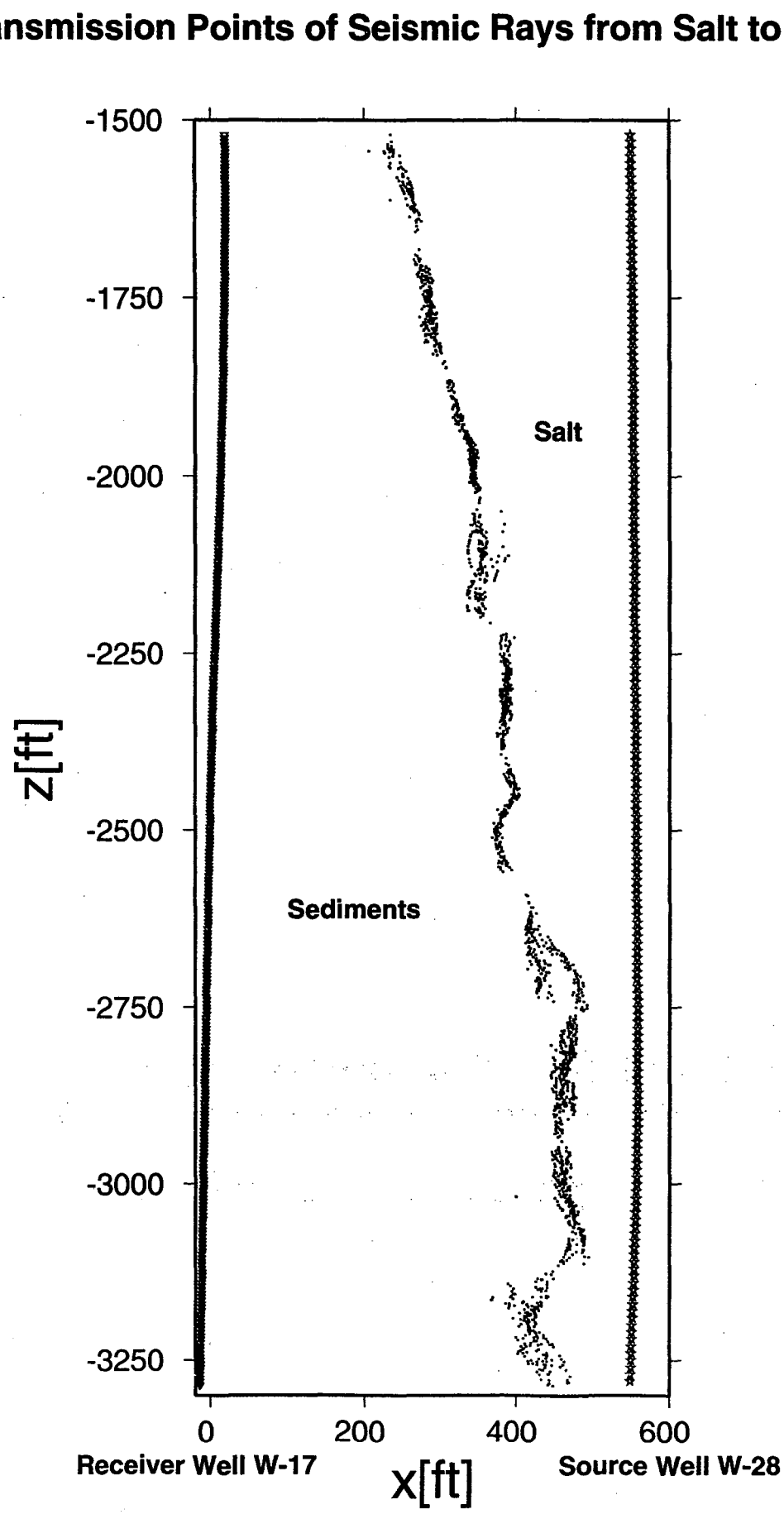

Figure 8 Location of salt-sediment interface estimated from crosswell survey between well 17 and well 28. Each dot represents the solution for one raypath.

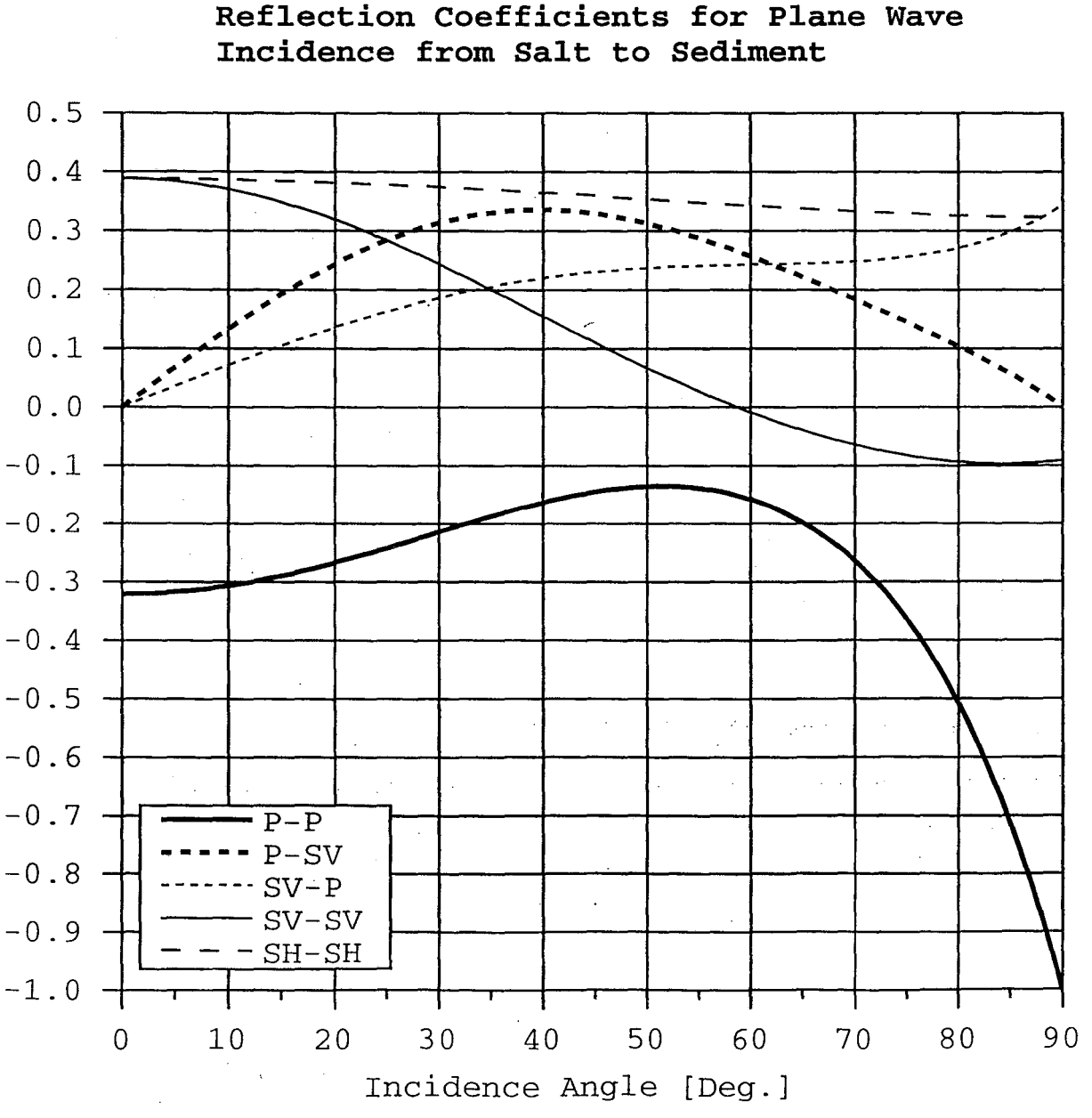

Figure 9a Reflection coefficients calculated from Zoeppritz's equations for a wave propagating in salt using velocities listed in text.

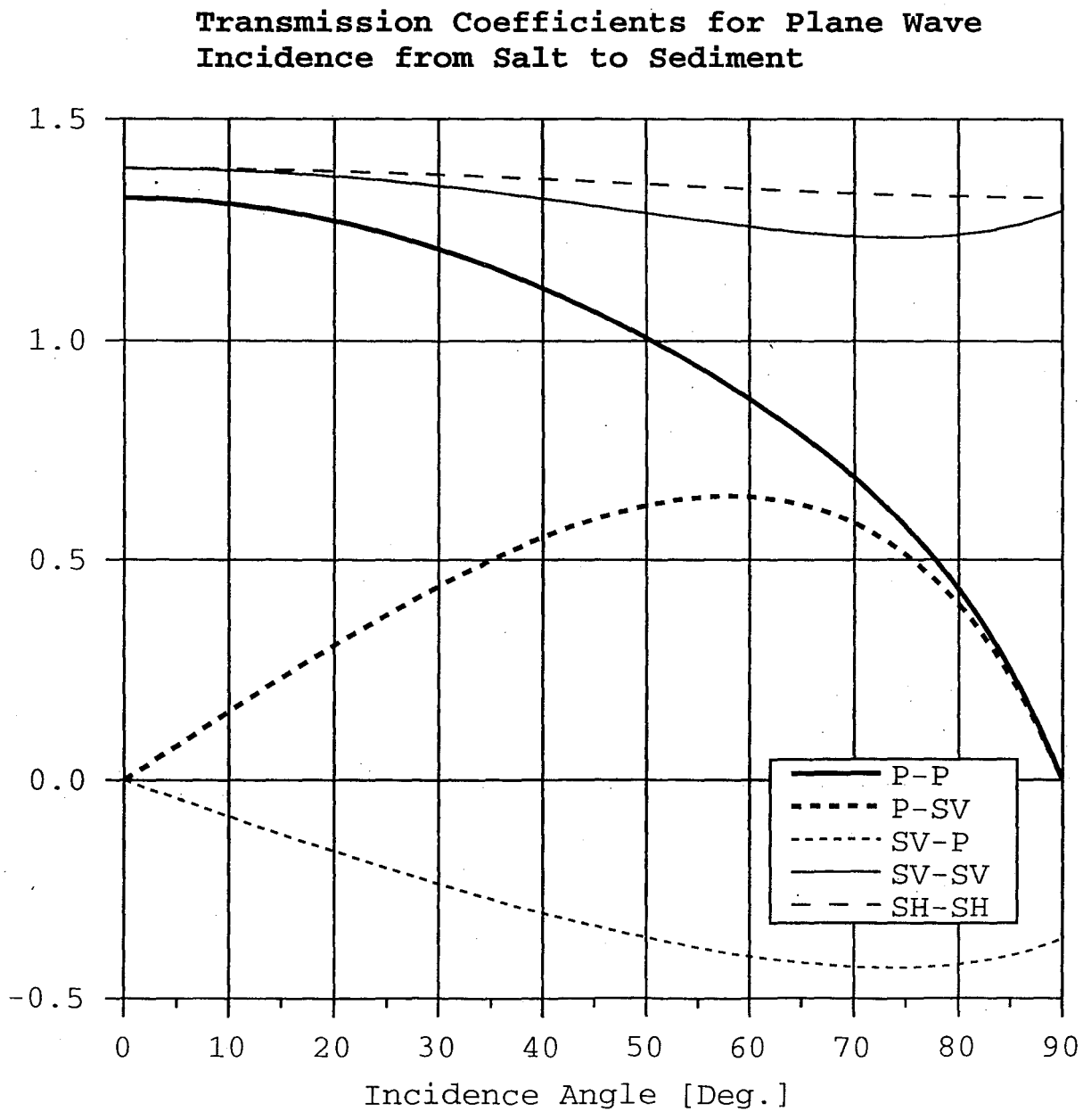

Figure 9b Transmission coefficients calculated from Zoeppritz's equations for a wave propagating in salt using velocities listed in text.

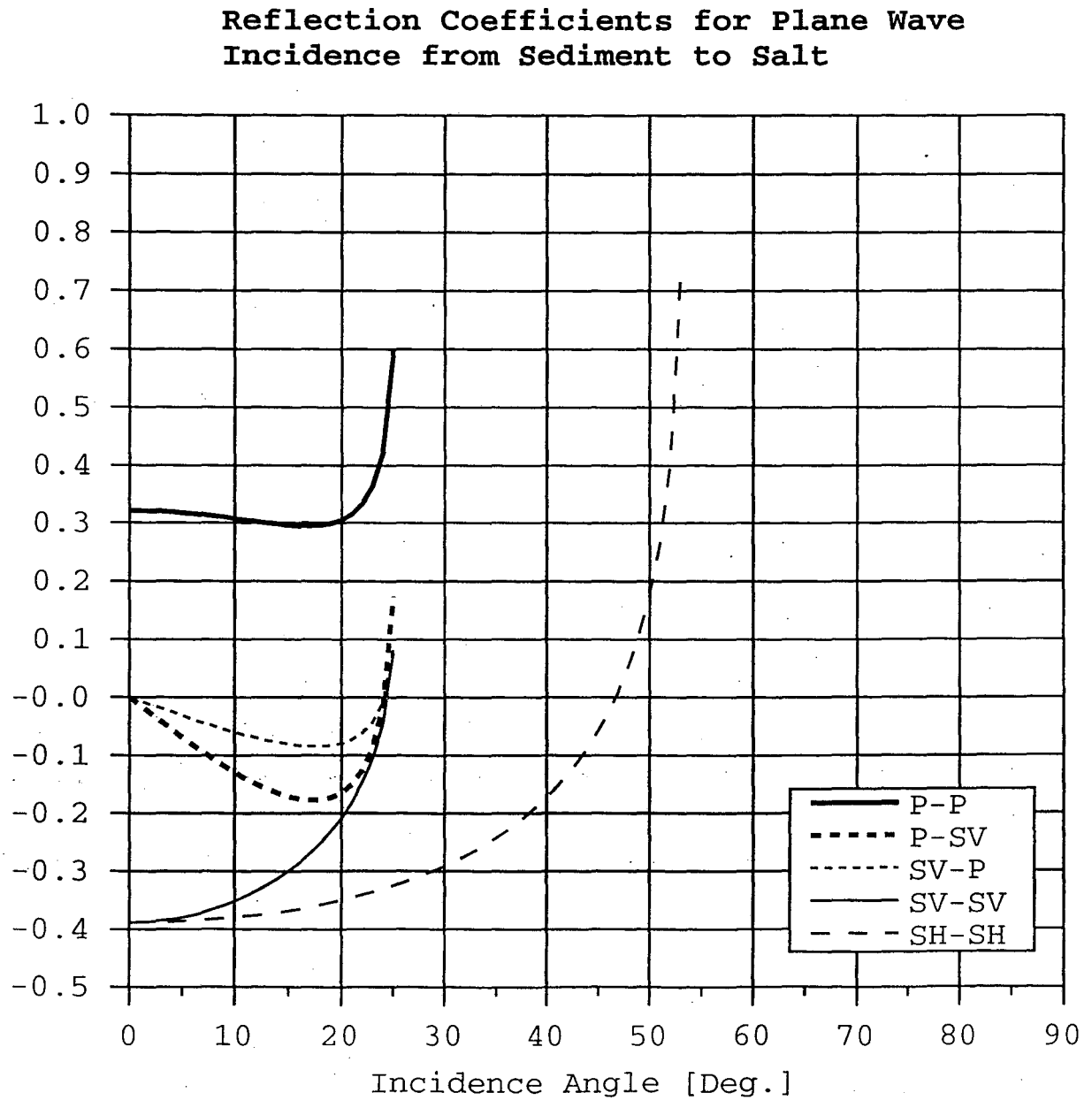

Figure 9c Reflection coefficients calculated from Zoeppritz's equations for a wave propagating in sediment using velocities listed in text.

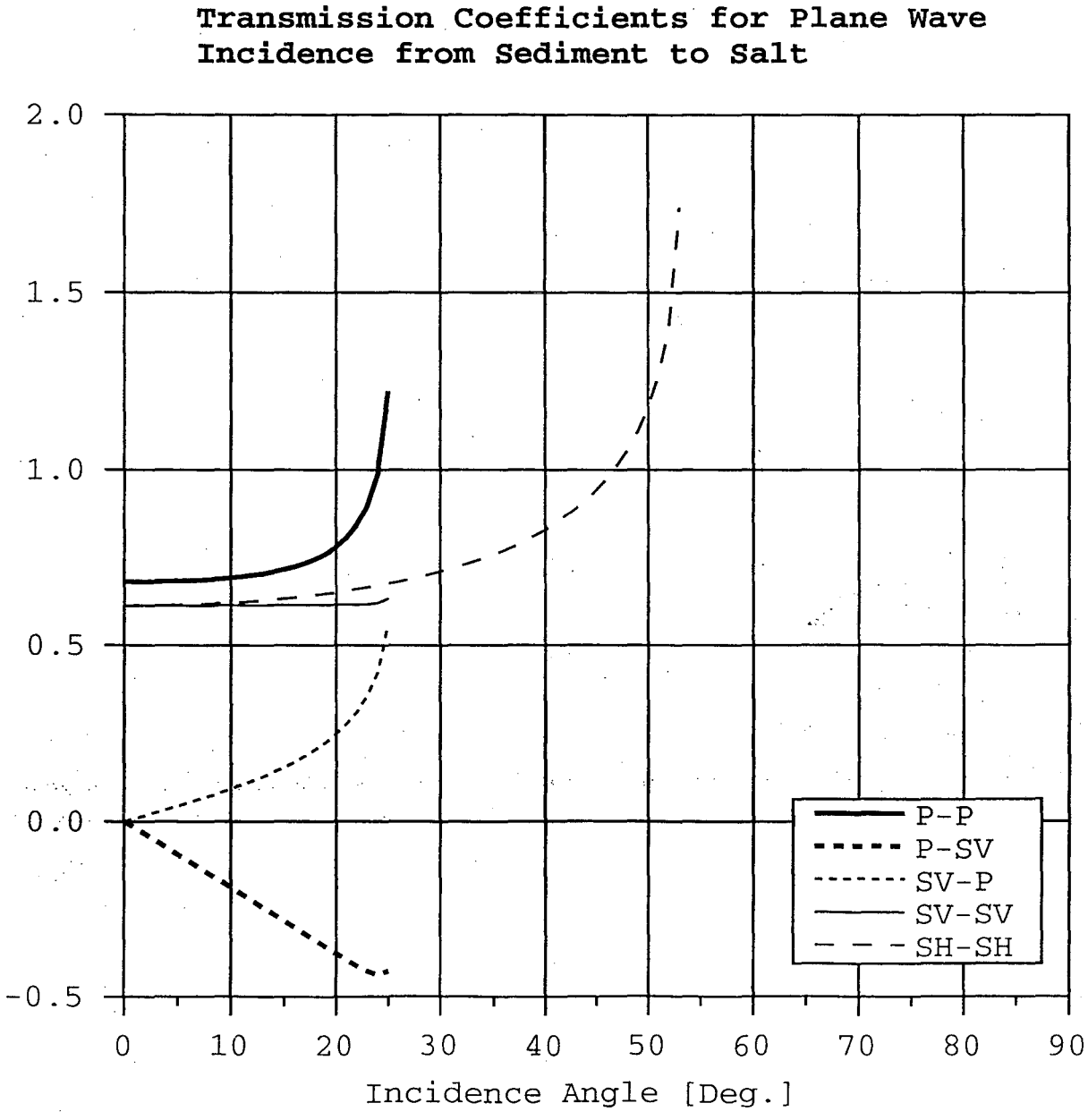

Figure 9d Transmission coefficients calculated from Zoeppritz's equations for a wave propagating in sediment using velocities listed in text.

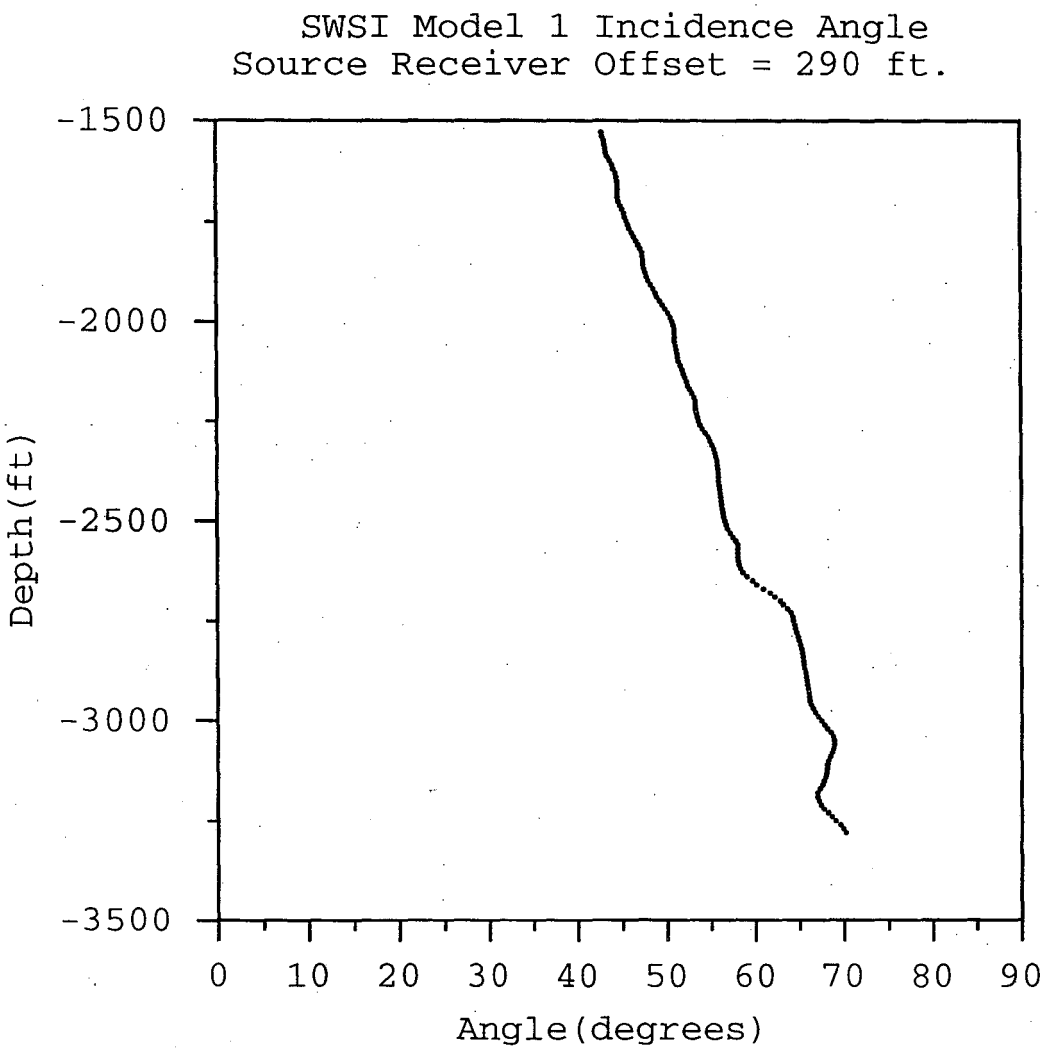

Figure 10 Incidence angle for a SWSI reflection in the salt for a source-receiver offset of 290 ft. using the model shown in Figure 8.

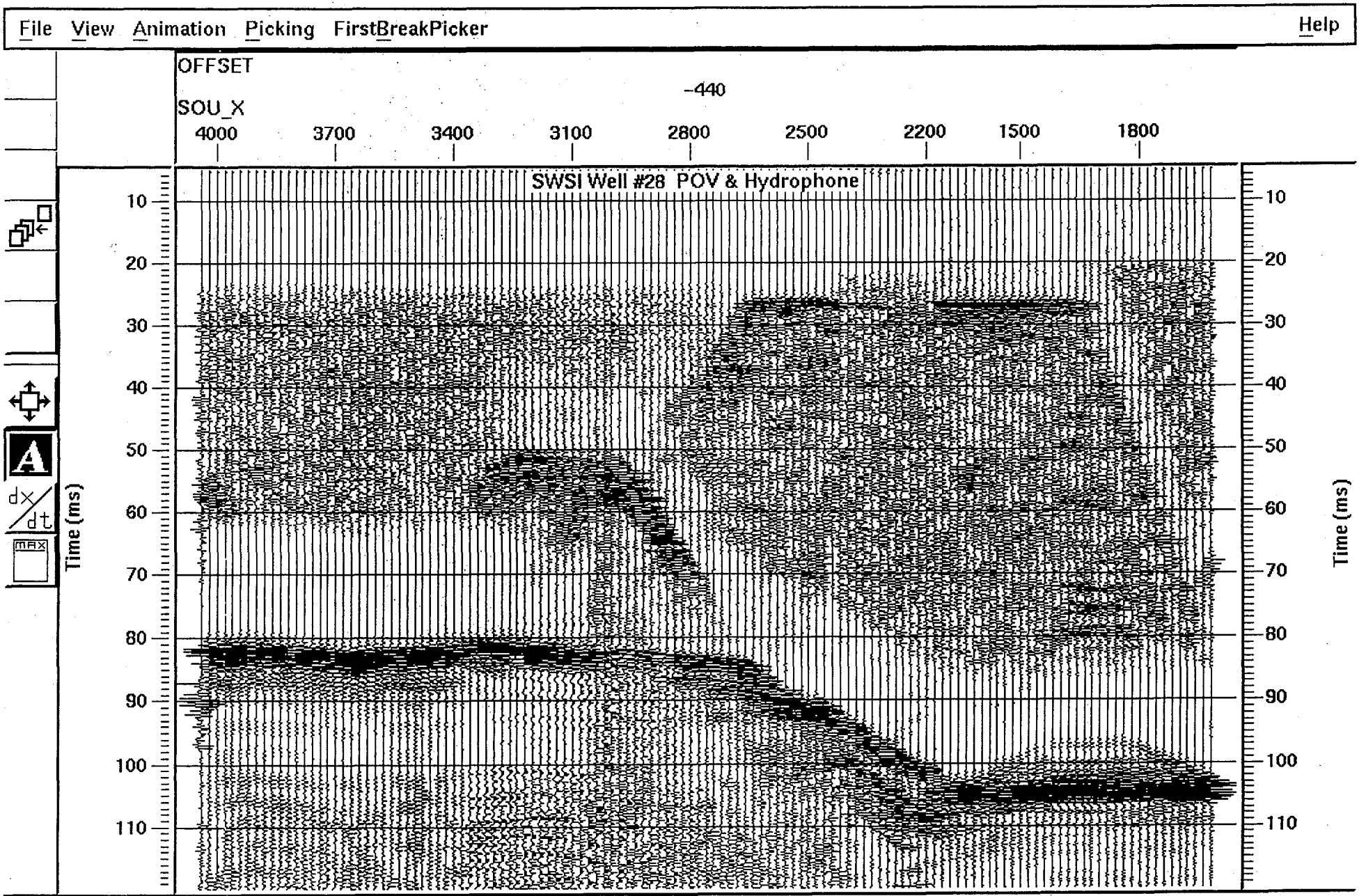

Print the screen to the printer.

Figure 11a Common receiver gather from well \#28 for the piezoelectric source (POV) and a hydrophone sensor with at 440 ft. source-receiver offset. a direct P-wave is observed at 27 ms, a direct S-wave is observed at 52 ms, and a tube-wave is seen between 80 and 110 ms. The change in tube wave travel time at 2600 ft.(source depth) is attributable to a change in borehole fluid from water to oil (Figure 2b) at 2850 ft.

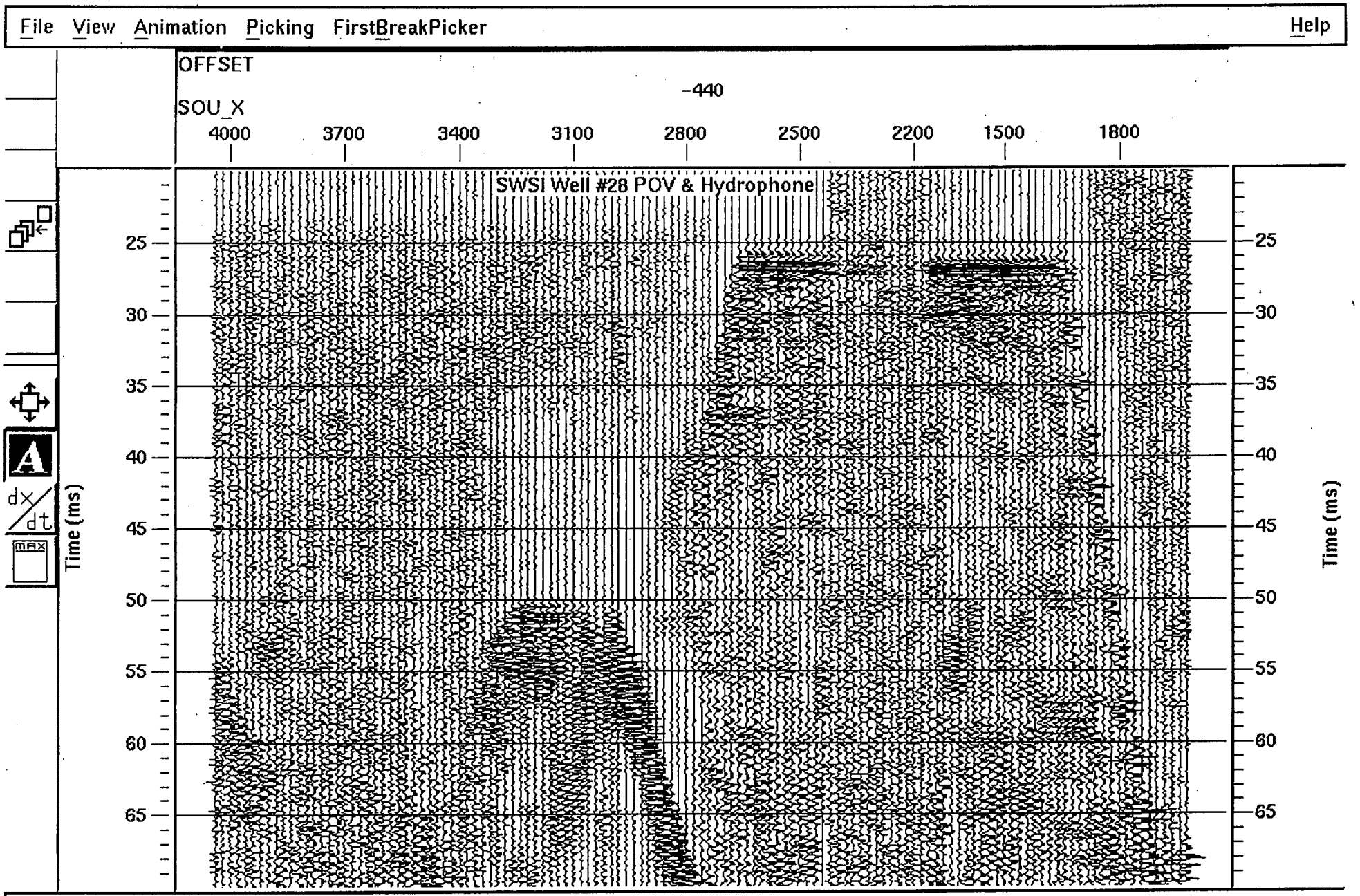

Print the screen to the printer.

Figure 11b Common receiver gather from well \#28 for the piezoelectric source (POV) and a hydrophone sensor with at 440 ft. source-receiver offset. a direct P-wave is observed at 27 ms, a direct S-wave is observed at 52 ms.

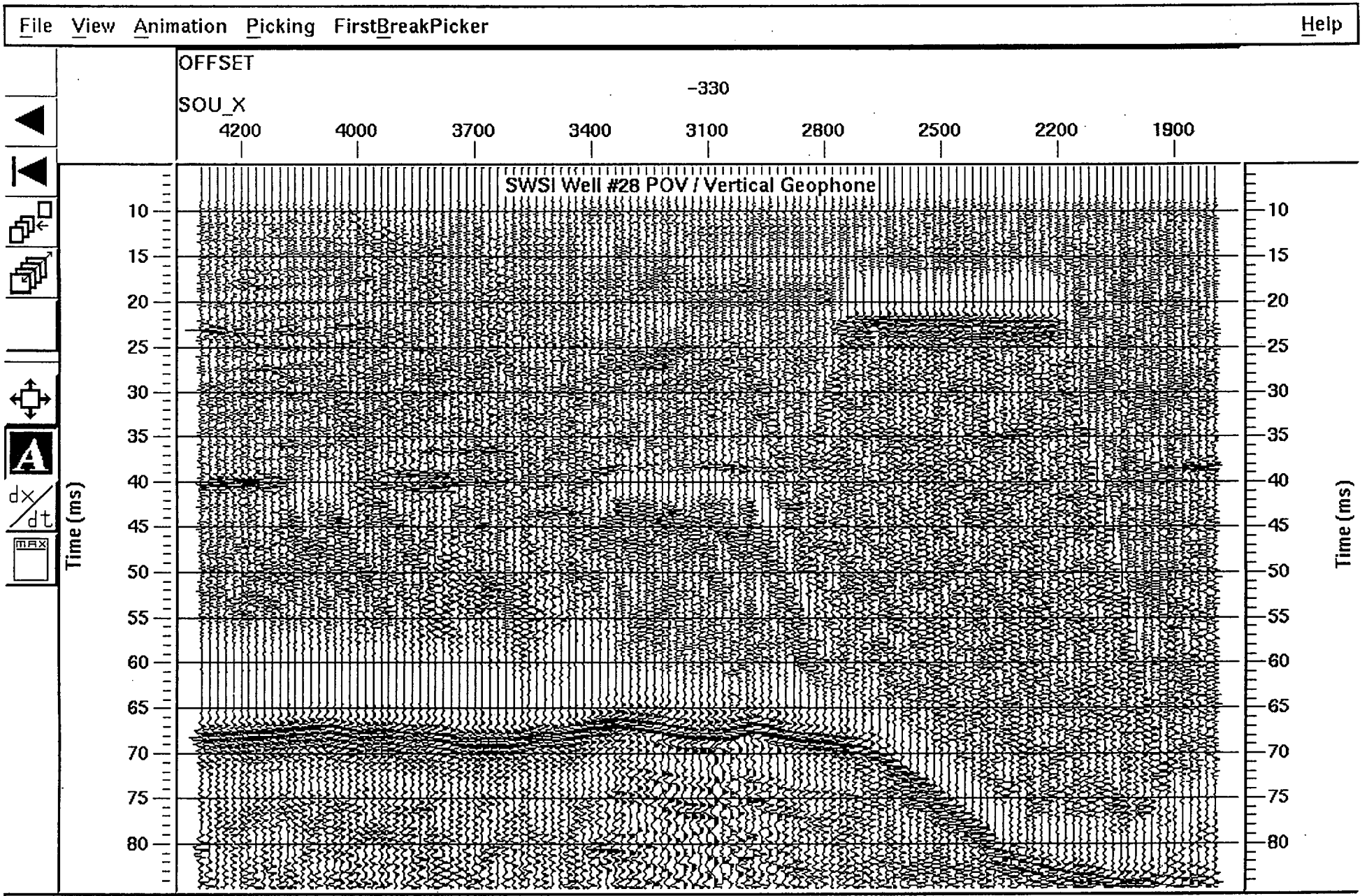

Print the screen to the printer.

Figure 12a Common receiver gather from well \#28 for a POV source and a vertical geophone with a 330 ft. source-receiver offset. A P-wave is seen at 23 ms and the tube wave is seen from 65 to 85 ms. A weak S-wave is seen between 40 and 45 ms.

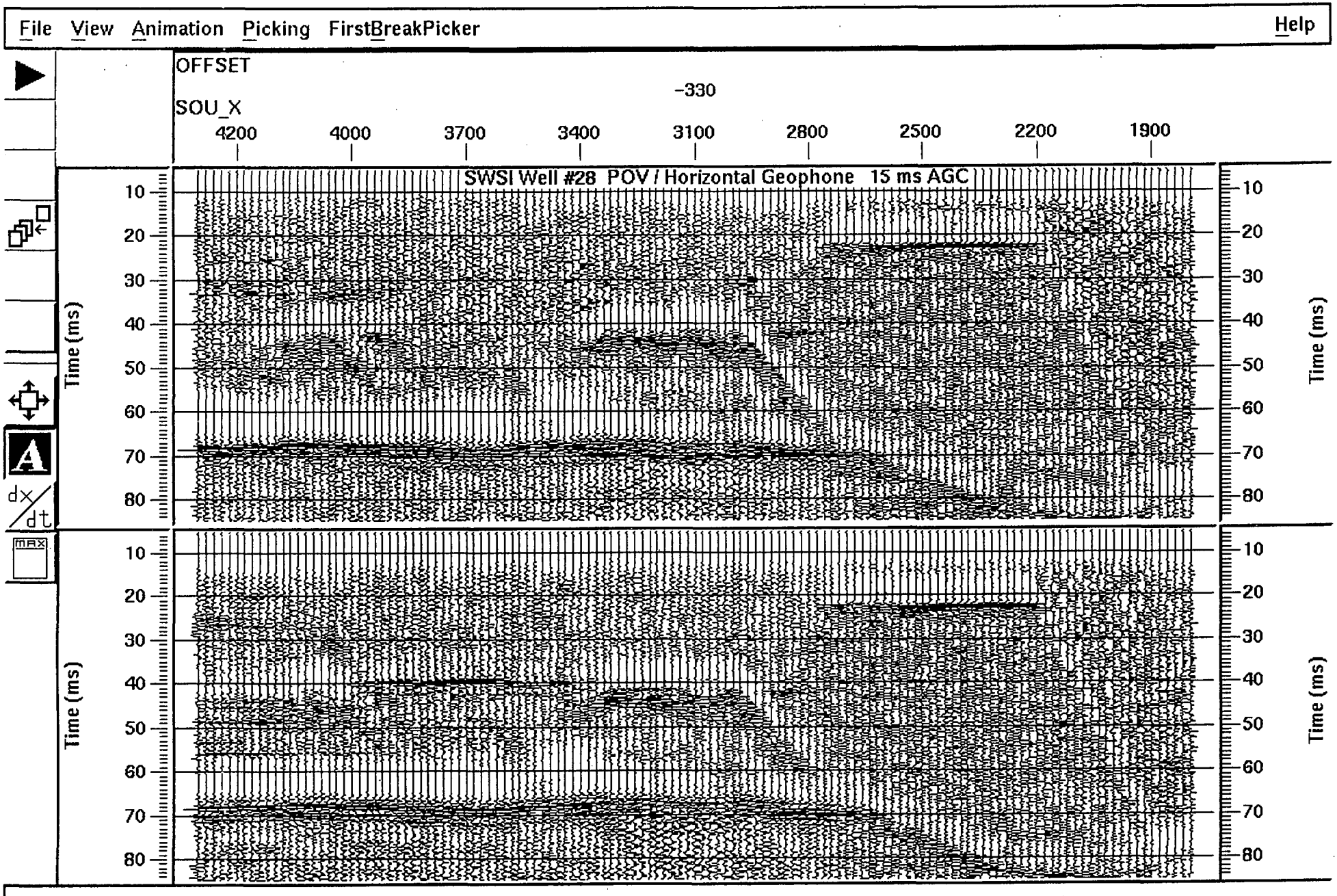

Print the screen to the printer.

Figure 12b Common receiver gather from well \#28 for a POV source and two horizontal geophones with a 330 ft. source-receiver offset. A P-wave is seen at 23 ms and the tube wave is seen from 65 to 85 ms. A weak S-wave is seen between 40 and 45 ms. S-wave energy is seen between 40 and 50 ms.

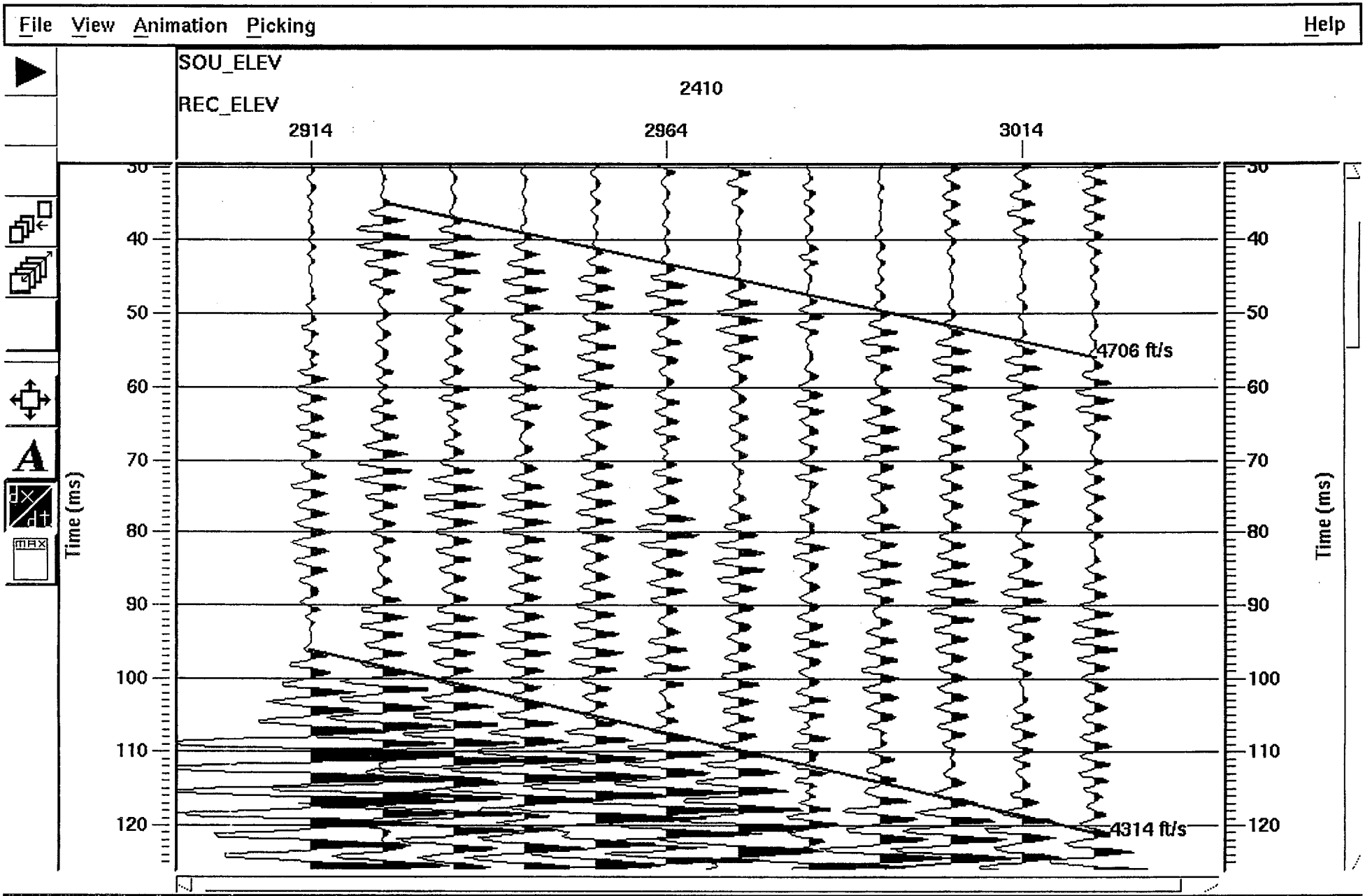

Print the screen to the printer.

Figure 13 Shot gather for well \#17 with orbital vibrator source and a geophone sensor. Tube wave "wrap around" noise is observed between 30 and 60 ms with a velocity of 4706 ft/s. The direct tube wave for this source-receiver offset (504 to 614 ft) is between 90 and 120 ms.

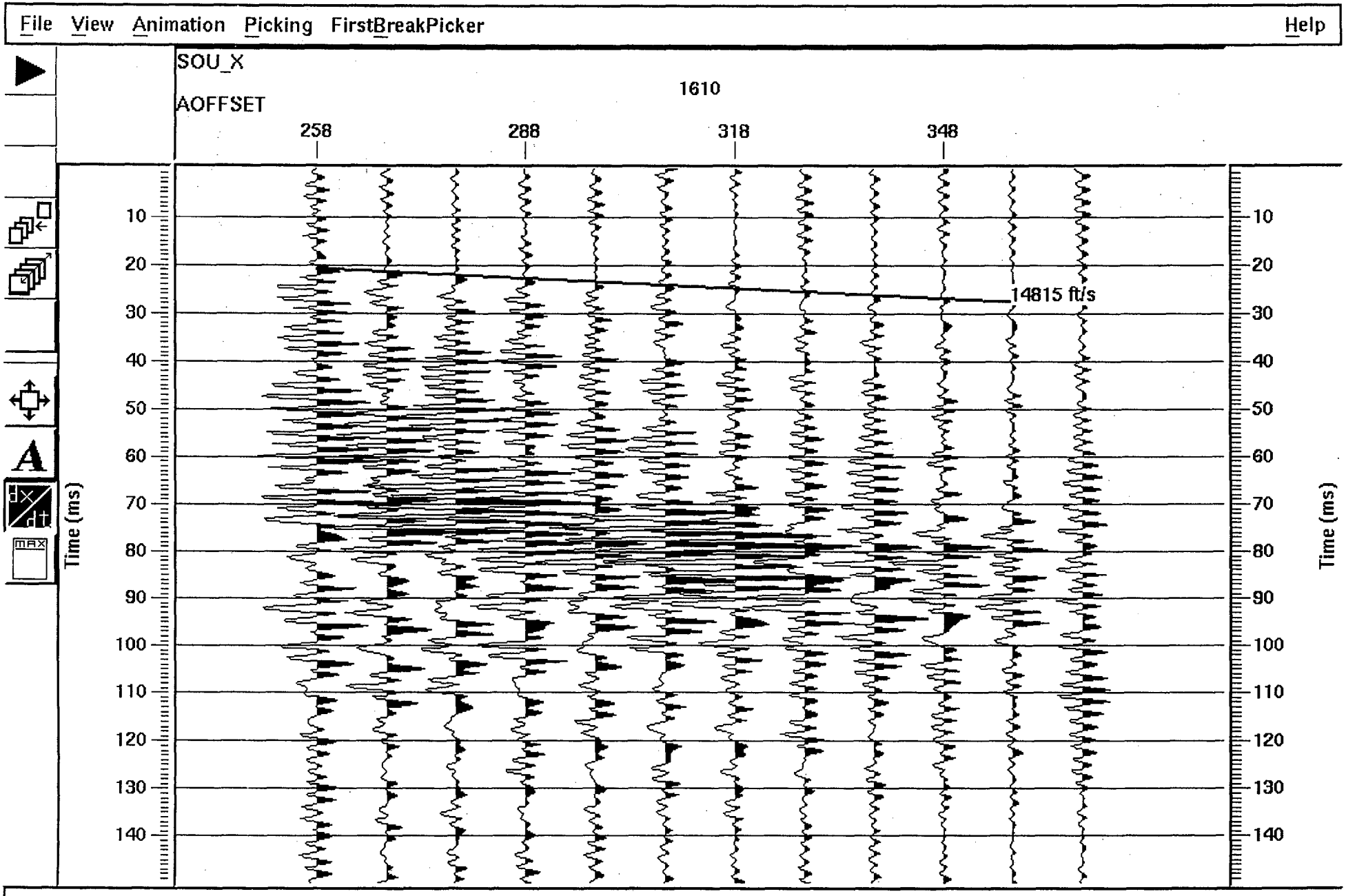

Print the screen to the printer.

Figure 14 Shot gather for well \#28 with orbital vibrator source and a geophone sensor. A direct P-wave arrival is shown with an estimated velocity of about 15,000 ft/s (the salt velocity).

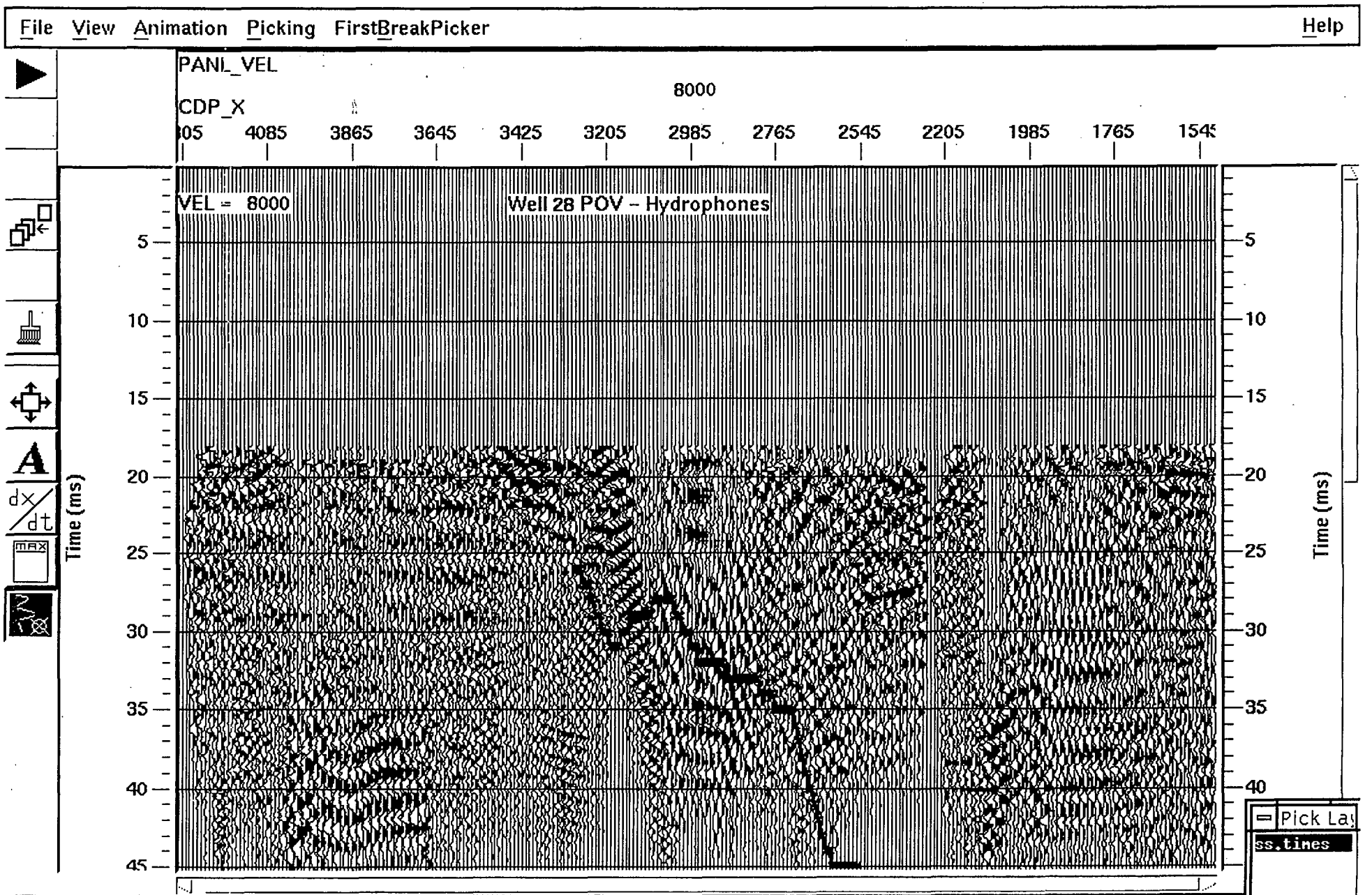

Figure 15a Constant velocity CMP stack of POV-hydrophone SWSI data from well \#28. The stacking velocity was 8000 ft/s (the estimated S-wave velocity in salt). The estimated arrival time of an S-to-S reflection is shown as dark line.

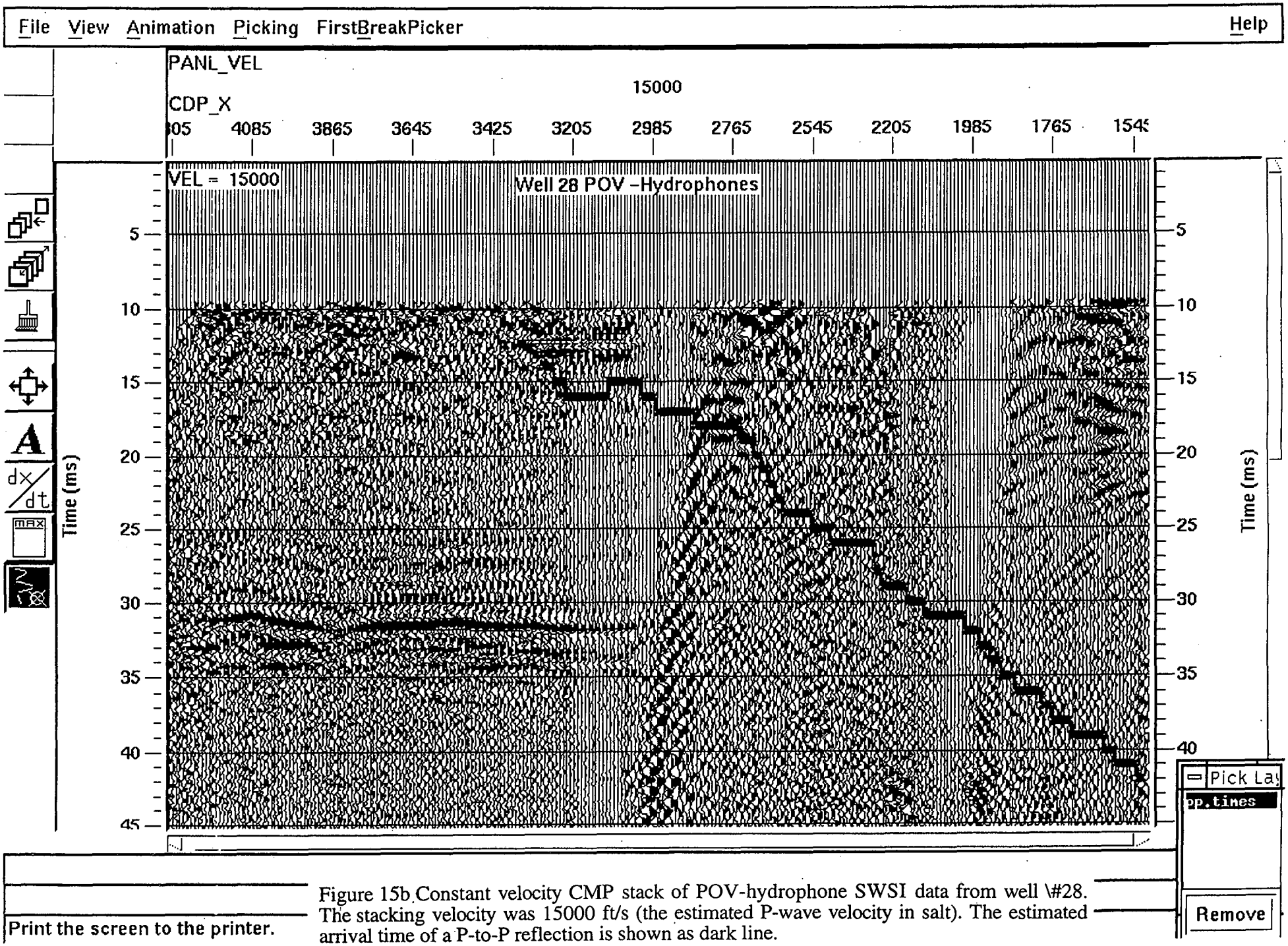

Figure 15b Constant velocity CMP stack of POV-hydrophone SWSI data from well \#28. The stacking velocity was 15000 ft/s (the estimated P-wave velocity in salt). The estimated arrival time of a P-to-P reflection is shown as dark line.

Print the screen to the printer.

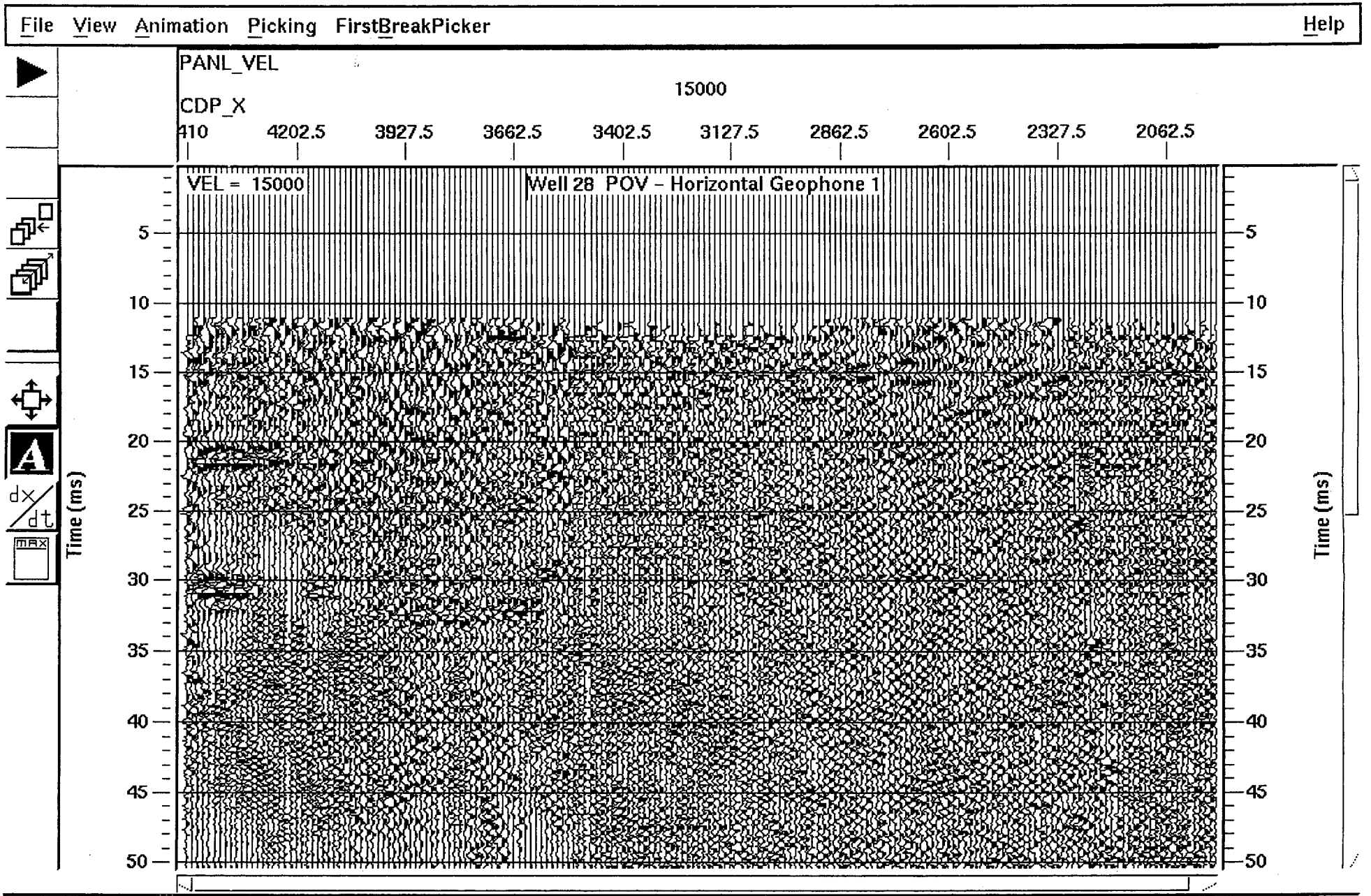

Print the screen to the printer.

Figure 16a Constant velocity CMP stack of POV-geophone SWSI data from well \#28 for horizontal 1. The stacking velocity was 15000 ft/s (the estimated P-wave velocity in salt).

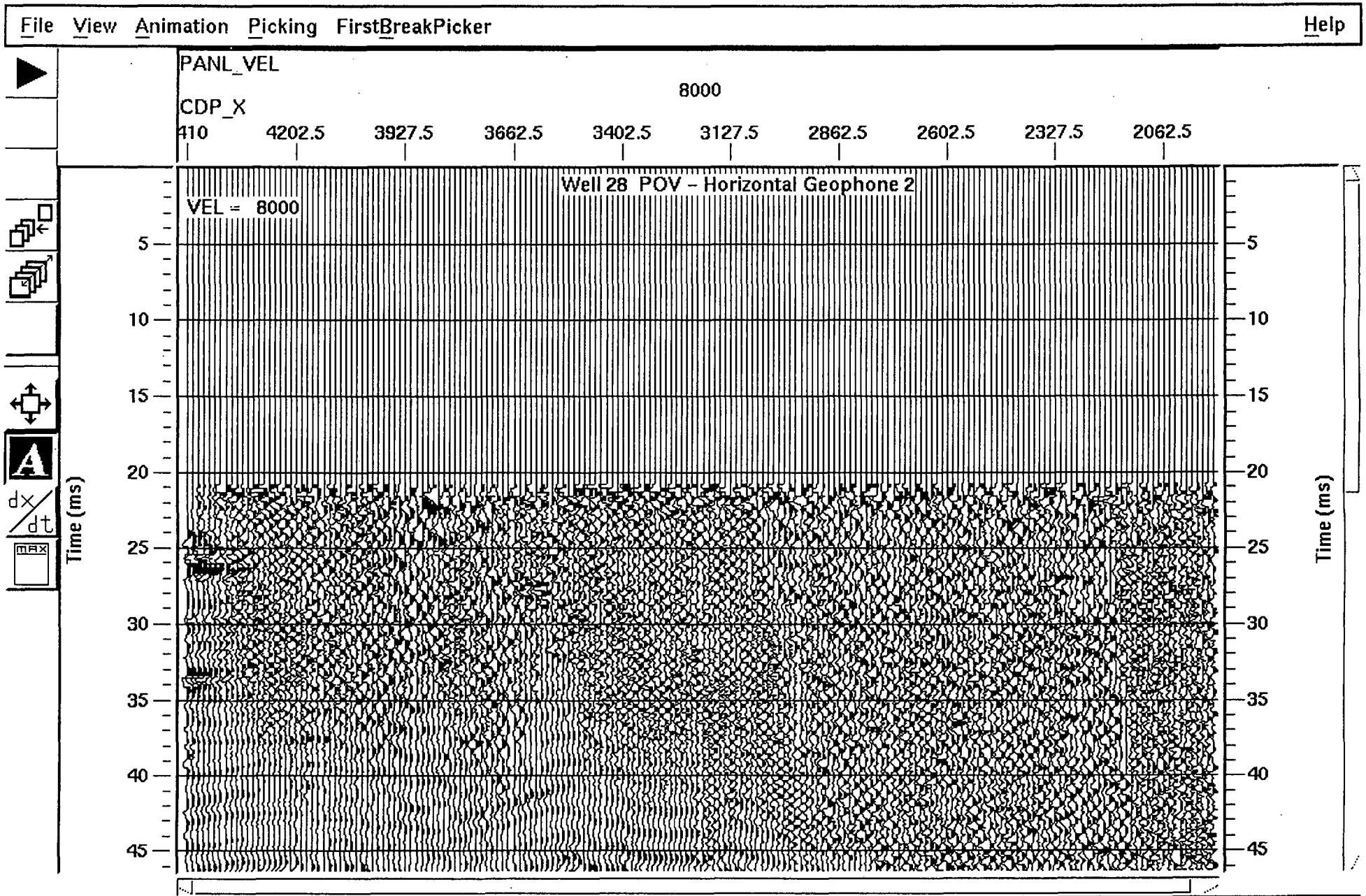

Figure 16b Constant velocity CMP stack of POV-geophone SWSI data from well \#28 for horizontal 2. The stacking velocity was 8000 ft/s (the estimated S-wave velocity in salt).

Print the screen to the printer.

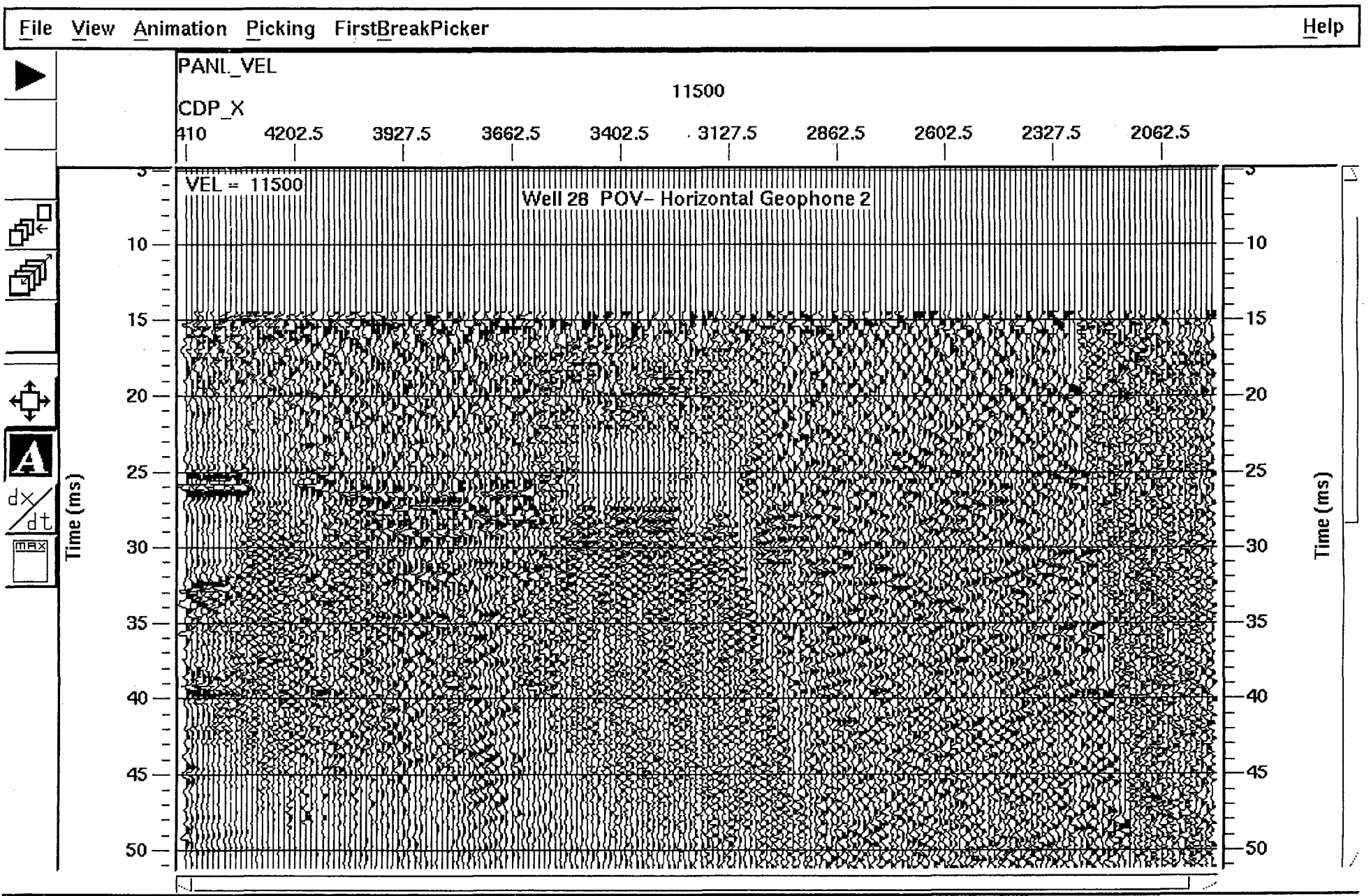

Print the screen to the printer.

Figure 16c Constant velocity CMP stack of POV-geophone SWSI data from well \#28 for horizontal 2. The stacking velocity was 11500 ft/s (the estimated average velocity for P-to-S conversions in salt).

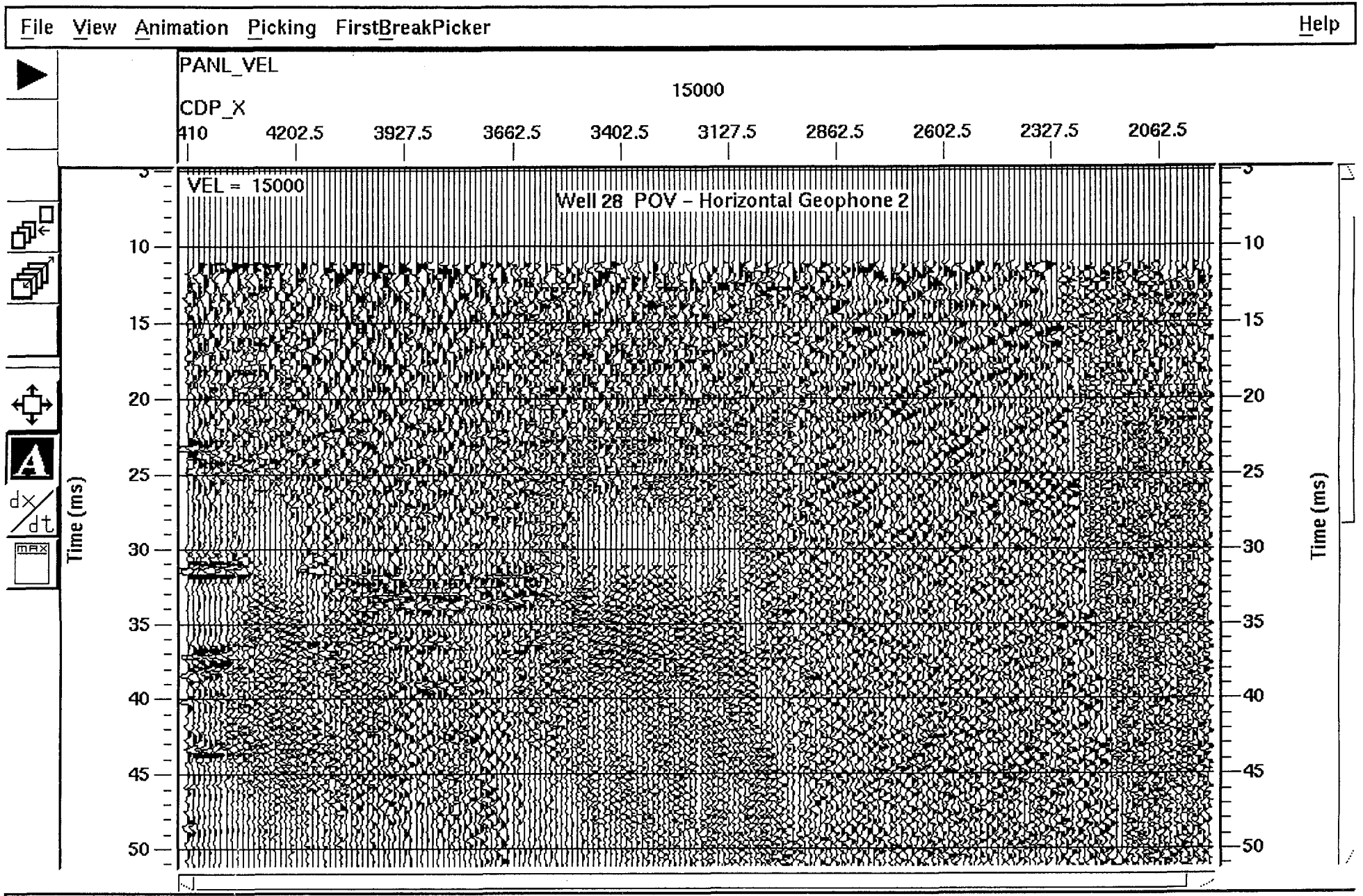

Print the screen to the printer.

Figure 16d Constant velocity CMP stack of POV-geophone SWSI data from well \#28 for horizontal 2. The stacking velocity was 15000 ft/s (the estimated P-wave velocity in salt).

Ernest Orlando Lawrence Berkeley National Laboratory
One Cyclotron Road | Berkeley, California 94720

Prepared for the U.S. Department of Energy under Contract No. DE-AC03-76SF00098